# UNIVERSITY OF MINES AND TECHNOLOGY

# TARKWA

FACULTY OF MINERAL RESOURCES TECHNOLOGY

DEPARTMENT OF GEOLOGICAL ENGINEERING

A THESIS REPORT ENTITLED

**PETROGRAPHY AND GEOCHEMISTRY OF METAVOLCANIC ROCK AND RELATED INTRUSIVES AND THEIR ALTERATIONS WEST OF BUTRE, GHANA**

**BY**

**VICTOR GRAHAM**

SUBMITTED IN PARTIAL FULFILLMENT OF THE REQUIREMENT FOR THE AWARD OF MASTER OF SCIENCE DEGREE IN GEOLOGICAL ENGINEERING

THESIS SUPERVISORS

| | |
|---|---|
| …… | …….. |
| DR G. M. TETTEH | PROF J. S. Y. KUMA |

TARKWA, GHANA

MAY, 2019

# DECLARATION

It is hereby declared that this thesis is as a result of research work undertaken by the author for the Master of Science Degree in Geological Engineering in the University of Mines and Technology (UMaT), Tarkwa, any aid, help or assistance obtained has been fully acknowledged. It should not therefore, in any form be it in part or whole be presented for another degree elsewhere.

……

(Signature of candidate)

Submitted this …… day of ……. (year)……..

# ABSTRACT

The metavolcanic rock and their related intrusives at Butre area in the Birimian Supergroup, southwest Ghana were studied to ascertain the mineralogical compositions, textures and metamorphism. The study showsthat the host rocks comprise of basalt and andesite whereas the intrusives are gabbroic diorite, diorite and granodiorite. The rocks are comagmatic emplaced in a subduction zone environment on a differentiation trend from tholeiitic basalt through gabbroic diorite, granodiorite, andesite and diorite. Intrusion of gabbroic diorite might have introduced arsenopyrite in the basalt whiles the diorite and granodiorite was accompanied by carbonate and pyrite. Amphibolite facies metamorphism was associated with garnet, epidote and magnetite whiles greenschist facies metamorphism was linked with epidote, chlorite, sericite, carbonate, pyrhotite and haematite. In general, all rock types are LREE depleted (La/Sm chondrite normalised ratios of basalt = 0.8 to 2.5; andesite = 2.03; diorite = 1.95 to 3.1; gabbroic diorite = 0.9 to 2.05; granodiorite = 1.66) with negative Eu and Ce anomalies. On the Alteration Index plot, the rocks show a general carbonatisation with sericite and chlorite alteration.

# DEDICATION

This work is dedicated to my parents Mr. and Mrs Graham, my siblings, Ms Linda Otchere and finally, Rev Fr G. N. Graham for their prayers, guidance and sacrifices made towards my education.

# ACKNOWLEDGEMENTS

Had it not been for your time, patience, guidance and advice, this work would not have been a success and for that reason, I say a big thank you to my supervisor Dr G. M. Tetteh. The lecturers of the department of Geological engineering especially Dr A. Ewusi, Dr K. Adomako-Ansah and Mr D. Aikins played important roles to make this work a success.

My entire family particularly my parents for their support and encouragement throughout my studies. Great thanks to Rev. Fr George Nelson Graham for his benevolence. Words alone cannot express my gratitude so I wish them abundant blessings and grace from God.

## TABLE OF CONTENTS

# LIST OF FIGURES

## LIST OF TABLES

# CHAPTER 1

## INTRODUCTION

### 1.1 Background

Granitoids in contact with host rocks are associated with different types of hydrothermal alterations, in most cases, accompanied by mineral deposits of economic value. For example, the Irizar granite of Kukri Hills, Antartica which was intruded by dolerite shows biotite altered to chlorite; and hornblende to chlorite and haematite along fractures (Craw *et al*., 1984). At Galore Creek of Canada, diorite/monzonitic intrusives has introduced hydrothermal potassic-calcic alteration in the surrounding host rocks (Micko *et al.*, 2014). In the Tavsanli area, Turkey, the Egrigöz granitoids intrusion into gneiss and schists caused silicification, argillic-sillicic, and phyllic alterations along fault/shear zones at the contacts of granitoids (Kumral *et al*., 2016). In Rajastan India, metavolcanic rocks intruded by granitoids have undergone mineralogical changes such as oligoclase to albite, and biotite to annite, with rocks unaffected by any hydrothermal event remaining intact (Kaur *et al*., 2012). Rajah *et al*. (1977) observed an inverse relationship between $Si_2O$ wt. % and oxides of Al, Mg, Mn, Ca and Fe but for $K_2O$ wt.%, the relationship was almost linear. Isocron diagram of least altered against altered rocks showed Nb and Th enrichment whiles Sr and Y were depleted after alteration (Derakhshani *et al*., 2009). The interaction of granitoids with host rocks are associated with different types of mineralisation including Cu-Au deposits (Micko *et al.*, 2014) and Sn deposits (Rajah *et al*., 1977).

The Birimian is a portion of the Man Shield, located south of the West African craton, comprising belts of metasedimentary (commonly slates, phyllites, greywacke) and metavolcanic (basalt, andesite, agglomerates, tuff) rocks disconnected by basins of sedimentary rocks (Leube *et al*., 1990). The age of the Birimian as estimated from zircons in the metavolcanics of the Birimian Supergroup shows ages between 2162 ± 6 Ma and 2266 ± 2 Ma, whiles detrital zircon grains from the metasedimentary rocks gave ages between 2180 and 2130 Ma (Oberthür *et al*., 1998; Perrouty *et al*., 2012). Three main types of granitoids are identified within the Birimian; volcanic belt type (Dixcove), K-rich (Bongo) and the sedimentary basin type (Cape Coast) granitoid type (Hirdes *et al*., 1992). Minerals of the volcanic belt type are non-foliated quartz and hornblende whiles K-rich granitoids are associated with hornblende and microcline which are also non-foliated (Kesse, 1985).

However, the sedimentary basin type is associated with well foliated biotite, microcline and beryl characterised by schist and gneiss enclaves (Perrouty *et al*., 2012). The two main types of granitoids identified in southern Ghana: volcanic belt type and sedimentary basin type according to (Leube *et al*., 1990) were emplaced at different times. Loh and Hirdes, (1999) stated that the age of belt granitoids in the southern portion of the Ashanti belt constrains the ages of the metavolcanic rocks that are in contact with these granitoids and since the belt granitoids occur within basalt of the volcanic belt, these rocks are considered comagmatic with ages between 2145-2190 Ma. Details of the sedimentary basin granitoids on the other hand suggest a late-to-post-kinematic but predates the Tarkwaian with ages between 2090-2125 Ma (Oberthür *et al*., 1995).

The Tarkwaian Group overlies the Birimian rocks of the Ashanti belt (Eisenlohr and Hirdes, 1992) as clastic sediments that were deposited at an approximated constrained age between 2102 and 2097 Ma (Perrouty *et al*., 2012) from metagabbro intrusives (Adadey *et al*., 2009) and granitoids (Oberthür *et al*., 1998). The Tarkwaian is sub-divided into the Kawere Series, the Banket Series, Tarkwa Phyllites and the Huni Sandstone which are intruded by dolerite and gabbro (Griffis *et al*., 2002). Within the Birimian, hydrothermal mineralisation in the basin granitoids is characterised by alterations which comprises quartz, sericite, calcite assemblages but diminishes gradually away from mineralised zone with albite, pyrite and chlorite assemblages (Smith *et al*., 2016). Alteration halos around mineralised zones at Obuasi mine is smaller (Yao and Robb, 2000) compared to that observed at the Julie deposit of Wa-East District (Amponsah *et al*., 2016 ). In Ghana, at the Mpohor area, SE of the Ashanti belt, intrusions of granodiorite and tonalite into sheared zones of the host rocks (gabbro and diorite) have led to the chloritisation of these host rocks (Tetteh and Effisah-Otoo, 2017). Also at the Prestea mine, SW of the Ashanti belt, alteration of pyrite to marcasite is common (Perrouty *et al*., 2012), whiles at Bekpong area, NW Ghana, intrusions have led to the chloritisation and sericitisation of shale (Amponsah *et al*., 2015 a).

Although a lot of work has been conducted in the southern part of Ghana (Sylvester and Attoh, 1992; Tetteh and Effisah-Otoo, 2017; Dampare *et al*., 2005; Eisenlohr and Hirdes, 1992), not much detailed work has been done in the study area. The alterations and textures with the geochemistry of the granitoids and metavolcanic rocks in the study area have not been studied in detail. Hence this work wished to explore the petrographic and geochemical relationship between the intrusives and their host metavolcanic rocks.

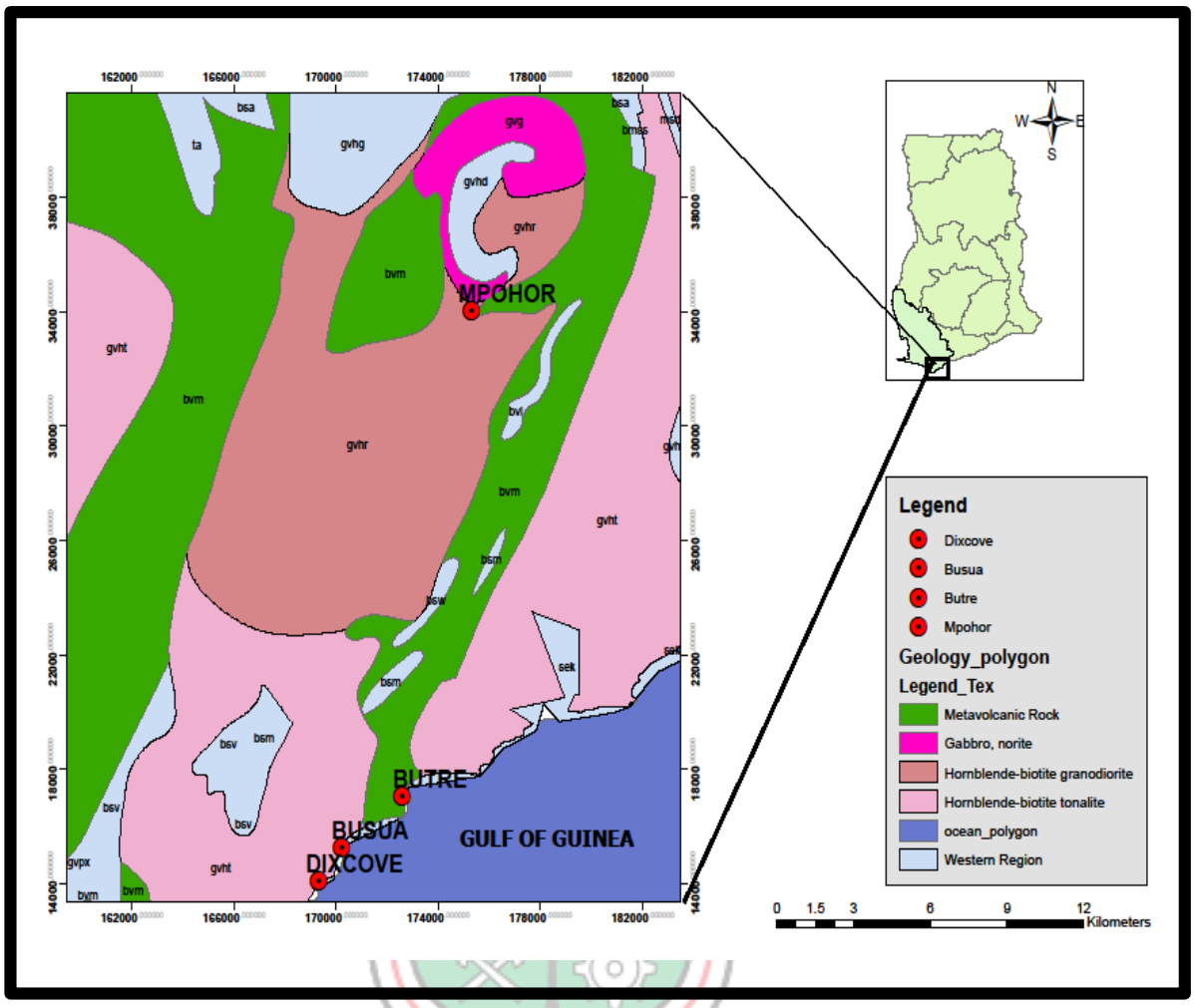


**Figure 1.1 Geological Map of southwest Ghana showing the Host Rock and associated Granitoids in the Study Area**

## 1.2 Thesis Objectives

The objectives of this study were to:

Sample the rocks west of Butre and show the variation of rocks near the granitoid-metavolcanic rock contact;

Study the petrography of the rocks for mineralogy, alteration types and metamorphism;

Study whole rock geochemistry of the rocks for major and trace element characterisation and

Deduce the tectonic setting of volcanism and check variations of alteration minerals.

## 1.3 Methods Used

Methods used in this study include;

a. Field sampling;

b. Petrography of thin and polished sections;

c. Sample analysis using XRF and ICP-ES and

d. Correlation of petrography with ICP-ES/ XRF data

e. Geochemical plots using GCDkit and Excel

## 1.4 Facilities Used

Facilities that were employed include;

Library and internet facilities at UMaT;

Leica DM 2700P microscope at Department of Geological Engineering, UMaT;

XRF and ICP-ES machines at the Associated Laboratory Services Minerals, Canada;

ArcMap, GCDkit and Deltagraph for geochemical plots and maps.

## 1.5 Chapter Outline

This thesis contains six chapters as follows:

- Chapter one gives the general introduction to some rocks in Ghana and other part of world with their alteration types, mineralisation as well as some mineralogical changes. This chapter also outlines the problem definition and the purpose of this study;
- Chapter two presents relevant literature to the study which include within its scope the regional and local geological setting of the study area;
- Chapter three outlines the methods and facilities that were used in the collection, processing and interpretation of data;
- Chapter four presents the results obtained from the study;
- Chapter five presents discussions of the results and

- Chapter six gives the conclusions of the study.

# CHAPTER 2

## LITERATURE REVIEW

### 2.1 Location, Accessibility and Physiography

Butre area falls within the Ahanta West District of Western Region, Ghana. It is located approximately 20 km southwest of Takoradi, the capital city of Western Region. The geographical coordinates are 30N 6020100 533201 and elevation of 115 ft (35 m). The road is tarred from Agona Township. Outside Agona Township towards Dixcove, the road becomes partially tarred and graveled. From Butre junction, which is off the Agona township-Dixcove road, the road is untarred all the way to Butre village. Figure 2.1 shows the geological map of the study area. Topography of the area is moderate with surrounding hills ranging from about 20 to 40 m above sea level and sheltered by forest between Busua and Asemkaw. Temperature is highest at $34^0$ between March and April and lowest at $20^0$ in August with relative humidity being 75 to 85% during rainy season and 70 to 80% on dry seasons. Rainfall is highest, 1700 mm between April and July which affects roads leading to the area, making accessibility difficult. The area is drained largely by the Butre River (which happens to be the largest river within the District) and to some extent, the Nana Pete lagoon. The area is also drained by. The drainage style is dendritic (branching) which helps improve soil fertility for agricultural purposes.

### 2.2 Geological Setting

The study area lies south of the Ashanti belt that is overlain by the Tarkwaian group and forms part of the Birimian supergroup. Hence a brief description and review of the Birimian supergroup, Ashanti belt and the Tarkwaian is important.

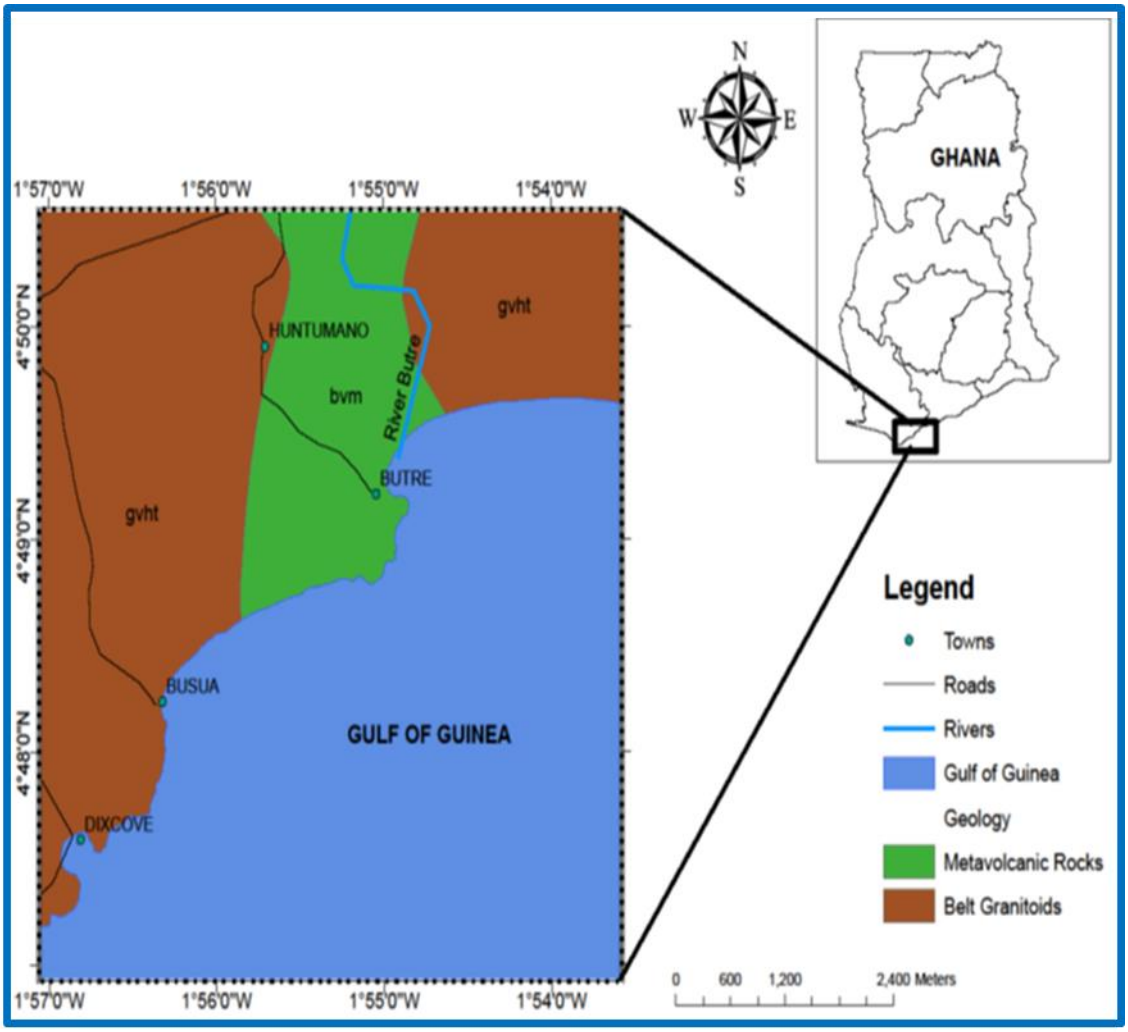


**Figure 2.1 Geological Map of southwest Ghana showing the Study Area**

### 2.2.1 Regional Geology

The West African Craton also known as the Guinea Rise is represented by rocks of lower Proterozoic timespan from 2500 to 1800 Ma. To the southernmost region lies the Man shield, made up largely of rocks of early Proterozoic age (Wright *et al.,* 1985). The Man shield is made up of Archean rocks of Liberian age (3.0-2.5 Ga) which lies to the west and an eastern portion made up of rocks of early Proterozoic age known as the Birimian rocks (Leube *et al.*, 1990). To the southeastern portion of the Man shield, the Birimian rocks outcrop, being extensive in La Côte d'Ivoire, Burkina Faso, Western Ghana, Southern Mali, West of Niger and Senegal (Abouchami *et al*., 1990). The Birimian of the Man shield has been folded, metamorphosed and intruded by various pluton suites (granitoids) and is believed to have occurred during the Eburnean age at 2.1 Ga (Leube *et al*., 1990).

The Birimian rocks of Ghana are composed of belts of metasedimentary and metavolcanic rocks that has been disconnected by basins of sedimentary rocks (Leube *et al*., 1990). The metasedimentary rocks of the Birimian are commonly made up of slates, phyllites, metagreywacke, tuffaceous shale, siltstone and Mn rich chemical sedimentary rocks (Eisenlohr and Hirdes, 1992). The metavolcanic rocks on the other hand are made up chiefly of basalt and andesite with interflow of some pyroclastic rocks (Loh and Hirdes, 1999). From zircon dating of the Birimian super group, the metavolcanic rocks gave ages between 2162 ± 6 Ma and 2266 ±2 Ma, whiles the metasedimentary rocks gave ages between 2180 and 2130 Ma (Oberthür *et al*., 1998; Perrouty *et al*., 2012).

Asihene and Barning, (1975) postulated that there is a break in stratigraphy between metavolcanic and metasedimentary rocks. However, Leube *et al*. (1990) is of the opinion that lateral facies occurs between metavolcanic and metasedimentary rocks of the Birimian in Ghana such that the metavolcanic belts and the metasedimentary with its subsequent sedimentary series occurring in the basins were deposited in the same time period. This assertion was later invoked and supported by Loh and Hirdes, (1999). Initially, Anglophone geologists were of the view that the metasedimentary rocks of the Birimian are older than the metavolcanic rocks. This idea was objected by the Francophone geologists who thought the reverse is true (Bessoles, 1977; Attoh, 1980). Amidst these opposing groups, Leube *et al*. (1990) proposed that it is possible that the metasedimentary and metvolcanic rocks may be related to each other in terms of origin.

The metasedimentary rocks (previously known as the lower Birimian) are composed primarily of phyllites and greywackes, which appear to change upwards to phyllites, metamorphosed tuffs, greywackes and felspatic sandstones. These series appear to grade conformably into the metavolcanic rocks (previously known as the Upper Birimian) which constitute basaltic and andesitic lavas with some rhyolitic and dacitic lavas (Wright *et al.*, 1985). Fig 2.2 sumarises the Birimian rocks of West Africa.

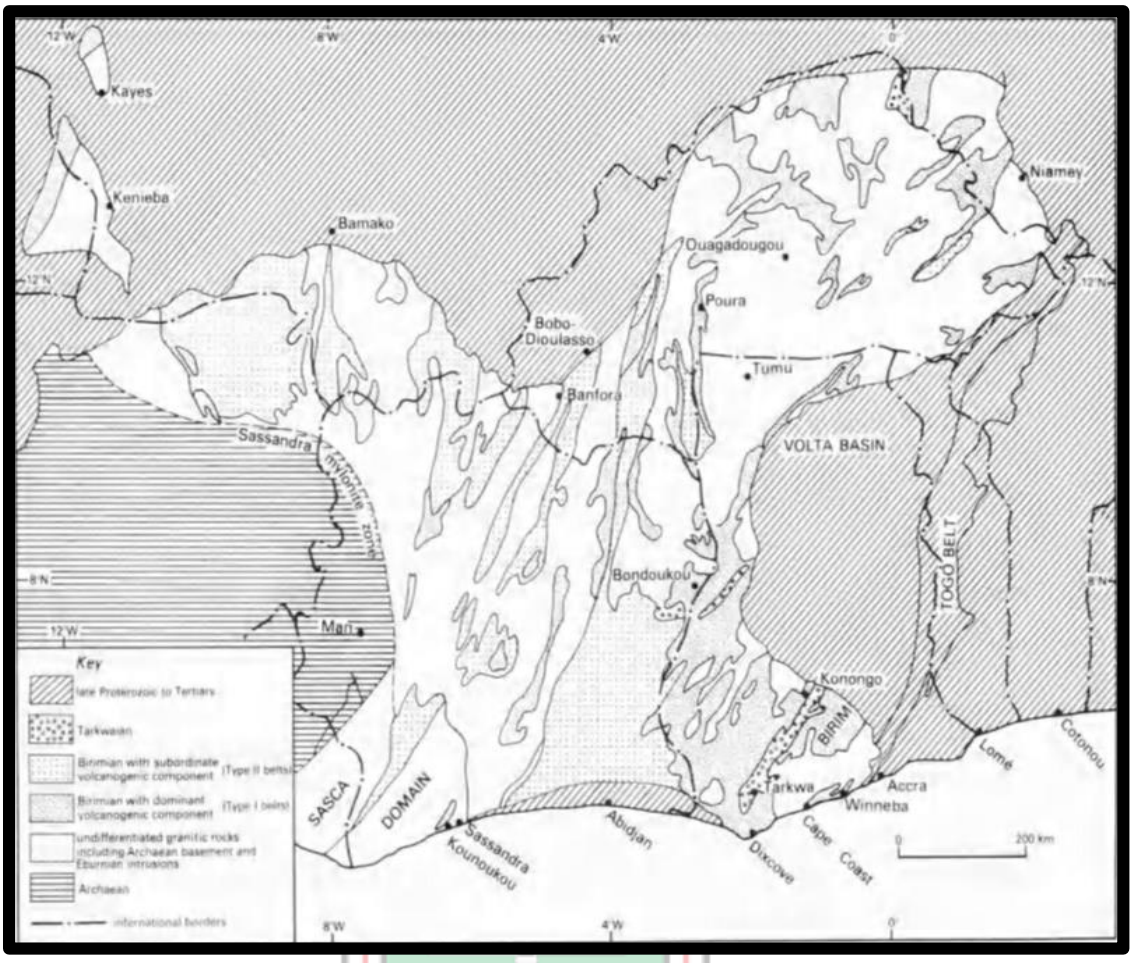


**Figure 2.2 Geological Map of West Africa showing Birimian Belts (after Wright *et al.*, 1985)**

In Ghana, the Birimian metasedimentary basins are located at the south-central (Cape Coast basin), southwestern (Kumasi and Sunyani basins) and the Northern (Maluwe) respectively (Smith *et al*., 2016). In southern Ghana, the basins are wide ranging from 60 to 70 km but narrows in the north (Griffis *et al*., 2002). Marginal to the belt are found various sedimentary rocks including wacke, turbidites, volcaniclastics, chemical sediments etc. (Hirdes *et al*., 1993). In general, the Birimian metasedimentary rocks progress into each other and divided into volcaniclastic rocks, turbidite related wacke,argillitic rocks and chemical sediments (Leube *et al*., 1990).

Given their depositional environment, these rocks are considered lithofacies such that the turbidite related wacke facies are observed at lower slopes of volcanic ridges. The argillite facies are located at the center of the basins whiles the chemical sediments are mostly found between volcanic belts and basins as transition zones. The associations of

volcaniclastic/argillite and argillite/volcaniclastics are seen close and away from volcanic ridges respectively (Griffis *et al*., 2002).

Birimian metavolcanic belts also known as the greenstone belts strike almost parallel to each other in a southwesterly to northeasterly direction and covers hundreds of kilometers. From Griffis *et al.* (2002), the belts have approximated widths of 20 to 70 km for larger belts and 10 to 20 km for smaller belts, which mostly occur in the north. There were previously six belts in the Birimian Supergroup of Ghana (Leube *et al*., 1990). However, Smith *et al*. (2016) outlined the following, named from southeast to northwest, Kibi-Winneba Belt; Ashanti Belt; Manso-Nkwanta-Asankragwa Belt; Sefwi Belt; Bui Belt; Bole-Navrongo Belt; Wa-Lawra Belt and Julie Belt as the major belts in Ghana. The formation and origin of the belts of the Birimian has been interpreted by various authors (Feybesse *et al*., 2006; Abouchami *et al.*, 1990; Berge, 2011; Sylvester and Attoh, 1992)

Tholeiitic lavas mostly of metamorphosed basalt and andesites are common within the belts together with some mafic rocks and interbedded dacite, rhyodacite and pyroclastics (Berge, 2011). Although lava/pyroclastic ratios are variable amongst the belts of the Birimian in Ghana, the highest ratios are observed in the Ashanti Belt whiles it is least in the Sefwi Belt (Leube *et al.*, 1990).

Berge, (2011) reported that the volcanic belts in Ghana holds tholeiitic lavas made up of basalt and andesite with interbedded felsic rocks such as dacite and rhyolite all of which have affected by metamorphism. At Labraboue of the Bromo greenstone belt Burkina Fasa, tholeiitic basalts are rare as they rather show calc-alkaline affirnity with signatures of arc magmatism (Beziat *et al.*, 1999). Abouchami *et al*. (1990) also reported that oceanic flood basalt, which had no continental influence evolved as deep plumes penetrating young lithosphere may have been the foundation of the tholeiites. Hence, the Birimian is seen to have evolved by arc volcanic followed by oceanic plateau concretions (Beziat *et al.*, 1999).

The Birimian of Ghana has undergone multiple deformations during the Eburnean regime at approximately 2130-1980 Ma (Perrouty *et al*., 2012) which is evident especially in the Ashanti Belt with six deformational events (D1 to D6) similarly recorded in other belts such as the Sefwi Belt (Perrouty *et al*., 2015). These deformational structures are observed to be the most controlling factor of gold mineralisation within the belts of the Birimian in Ghana

and even, the Tarkwain (Griffis *et al*., 2002). Hirdes *et al*. (1992) reported three types of granitoids occur within the Birimian of Ghana namely; Sedimentary Basin type, previously referred to as Cape Coast granitoids; volcanic belt type previously as Dixcove granitoids and K-rich (Bongo) granitoids, however, the first two are the main types of granitoids identified in southern Ghana and are of Paleoproterozoic age (Griffis *et al*., 2002; Yao *et al*., 2001). Minerals of the volcanic belt type are non-foliated quartz and hornblende, whiles K-rich granitoids are associated with hornblende and microcline, which are also non-foliated (Kesse, 1985). However, the sedimentary basin type is associated with well foliated biotite, microline and beryl characterised by schist and gneiss enclaves (Perrouty *et al*., 2012). Belt granitoids occur within basalt of volcanic belt and hence are considered comagmatic with ages between 2145-2190 Ma whiles, the basin-type is regarded as late-to-post-kinematic and predate the Tarkwaian with ages between 2090-2125 Ma (Oberthür *et al*., 1995). Whereas the belt types are smaller in size, the basin types are larger and occur as batoliths in the sedimentary basins. The former is older and associated with the volcanic belts (Griffis *et al*., 2002). It is believed that the belt type granitoids resulted from subduction setting and show close resemblance with tonalite-trondhjemite-granodiorite granit (TTGs) (Tapsoba *et al*., 2013; Grenholm, 2011). Beziat et al. (1999) believe these granitoids were derived from slab melting and deposited in a subduction environment, which could be the reason for their calc-alkaline features and mantle interaction signatures. The basin granitoids on the other hand formed as a result of crustal anatexis which accompanied the Eburnean orogeny but may have taken place in transverse deformation zones in an aqueous environment. (Grenholm, 2011). These granitoids were classified by Yao *et al*. (2001) as either mineralised or unmineralised. Other mafic intrusions are also present in the Birimian occurring mostly in the volcanic belts; the Ashanti and Sefwi Belts habouring the most (Griffis *et al*., 2002). Griffis *et al*. (2002) also believe that these mafic intrusives pre-dates the metamorphism of the volcanic belts but, they post-date the belt granitoids in appearance. Fig. 2.3 summarises the major belt granitoids of Ghana.

In Ghana, the Tarkwaian Group overlies the Birimian rocks and is perceived as fragments of the Birimian that uplifted and eroded after the Eburnean Tecto-Thermal Event (Eisenlohr and Hirdes, 1992). Junner *et al*. (1992) believes the Tarkwaian is a supracrustal system of Proterozoic age. The Tarkwaian is much matured within the Ashanti and the Bui Belts with approximated thickness of 2500 and 9000 m, respectively (Griffis *et al*., 2002).

The age of the Tarkwain as estimated from metagabbro intrusions and granitoids gave 2102 and 2097 Ma (Perrouty *et al*., 2012; Adadey *et al*., 2009 and Oberthür *et al*., 1998) and is sub-divided into the Kawere Series, the Banket Series, Tarkwa Phyllites and the Huni Sandstone which are intruded by dolerite and gabbro intrusives (Griffis *et al*., 2002).

The Tarkwaian is observed as less deformed and metamorphosed than the Birimian rocks giving rise to a strong unconformity. However, in other places where the Tarkwaian outcrops, these signatures are absent (Wright *et al*., 1985). Elsewhere in other regions of the Birimian such as Côte d'Ivoire and the Upper Volta (Burkina Faso), the Tarkwain rocks contain volcanic pebbles and mica-schist pebbles in the conglomerates. This makes the Geologists in this region to believe that the volcanic and sedimentary rocks of the Birimian of Ghana are of lateral facies and that there was deformation, metamorphism and erosion in some places between these facies (Wright *et al.*, 1985).

### 2.2.2 Local Geology

Butre area lies on the far south of Ashanti Belt within the Birimian metavolcanic portion (Fig 2.1). This part of the belt is composed of volcanic rocks of mainly metamorphosed basalt and andesite together with pyroclastics and sedimentary rocks and have been intruded by granite-diorite suites (Dampare *et al*., 2008). There also occur mafic-ultramafic intrusives of various sizes, the largest having been described by Attoh *et al.* (2006) as complex ophiolite of Paleoproterozoic age and occurs in a supra-subduction zone. Allibone *et al*. (2002a) agrees with other authors such as Oberthür *et al.* (1998) and Davis *et al*. (1994) that both the volcanic belt and the sedimentary basins evolved at two separate orogenic cycles named as Eburnean 1 and 2 and summarised as follows:

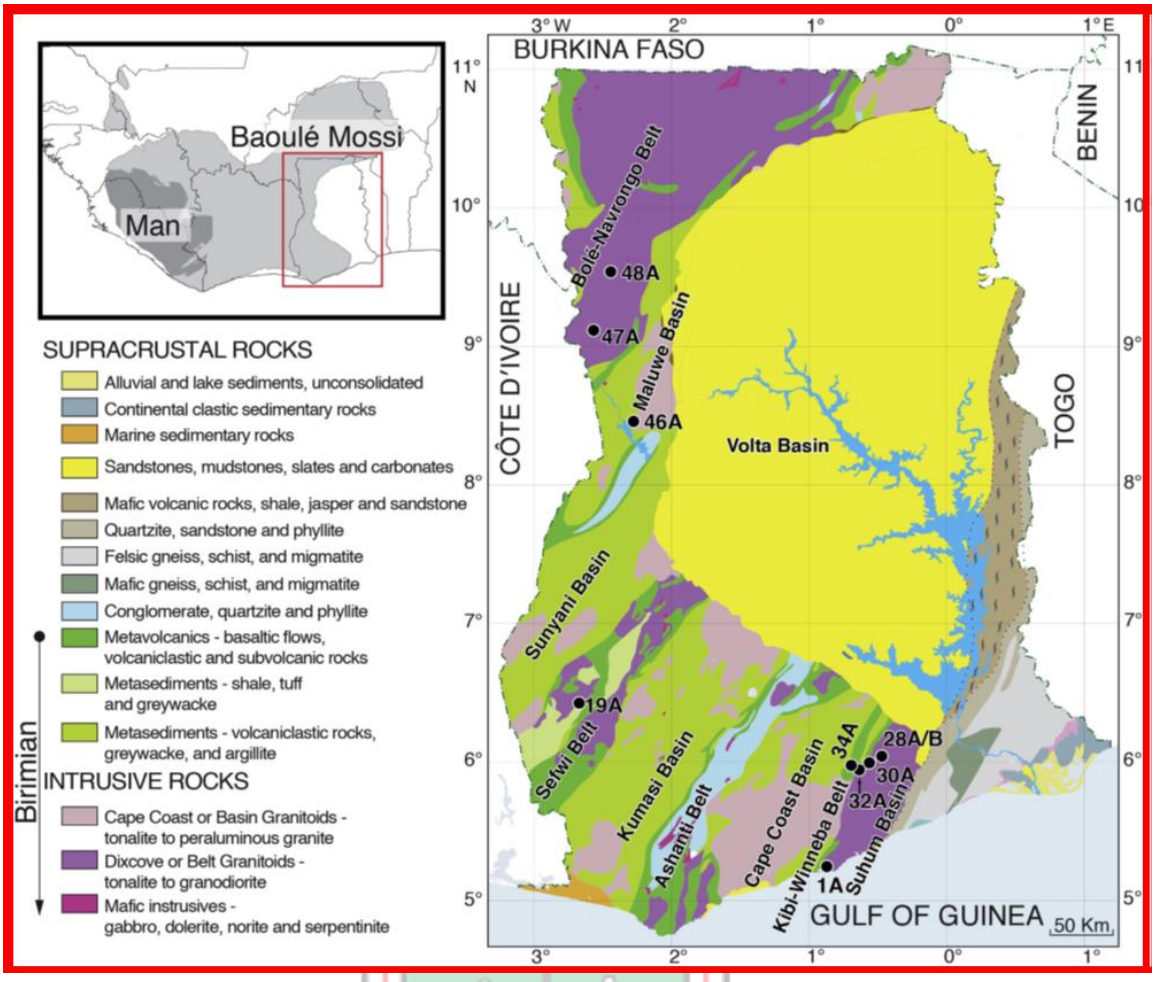


**Figure 2.3 Geological Map of southwest Ghana showing major Belts and Basins (after, Petersson *et al.*, 2018)**

- Eburnean 1 event which approximately occurred between 2240 - 2150 Ma initiated the magmatic eruption of the Birimian volcanic rocks followed by intrusions (granitoids) that cut the earlier volcanic rocks, which in turn led to period of metamorphism followed by uplift and erosion;
- Eburnean 2 event at approximately between 2130 – 2088 Ma was responsible for the deformation and metamorphism of the Birimian rocks to lower greenschist facies together with the Tarkwain (Allibone *et al*., 2002a).

At Butre area, the metavolcanic rocks of the Birimian include the pillow basaltic lavas. These rocks are in contact with three granitoids namely: tonalite in the south, granodiorite in the centre and gabbro/norite at the northern part of Mpohor town. Xenoliths present in tonalite are considered to be contact metamorphosed, metasomatised basaltic rocks (Loh

and Hirdes, 1999). Metamorphism to amphibolite facies was observed in the rocks especially at areas in proximity to granitoids (John *et al*., 1999).

# CHAPTER 3

## METHODS USED

### 3.1 Resources and Methods Used

Samples were collected from Butre area (Fig 2.1) for petrographic and geochemical analysis to give a good representation of the various rock types. Sampling was across intrusive/metavolcanic rock contact and all samples were collected from fresh rocks such that much information could be taken.

In all, thirteen (13) representative samples were collected from the study area. All samples were described in hand specimen. Thirteen (13) thin and polished sections were prepared from fresh rock samples and studied under transmitted and reflected light microscopy to ascertain the minerals and their properties at the Petrology Laboratory of the Geological Engineering Department, University of Mines and Technology UMaT, Tarkwa. Appendix C outlines the number of samples collected and their GPS coordinates.

Thin sections were prepared based on procedures summarised in Hutchison (1974). The sections were studied using the Leica DM 2700P microscope. Mineral identification was founded on mineral characteristics such as their colour, texture, pleochroism, bireflectance and anisotropy. Whereas modal percentages were done by point counting, mineral abbreviations were after the criteria of Schmid *et al.* (2007).

Opaque minerals in thin sections were studied in details in polished sections using the Leica DM 2700P microscope. These minerals were identified and characterised based on their textural relationship taking into account mineral associations and alteration. These identification and textural relationships were aided by the criteria of Deer *et al.* (1966) and Verma (2010). QAP diagrams were plotted after normalisation of modal percentages. Sample locations are summarised in (Fig. 3.1) below.

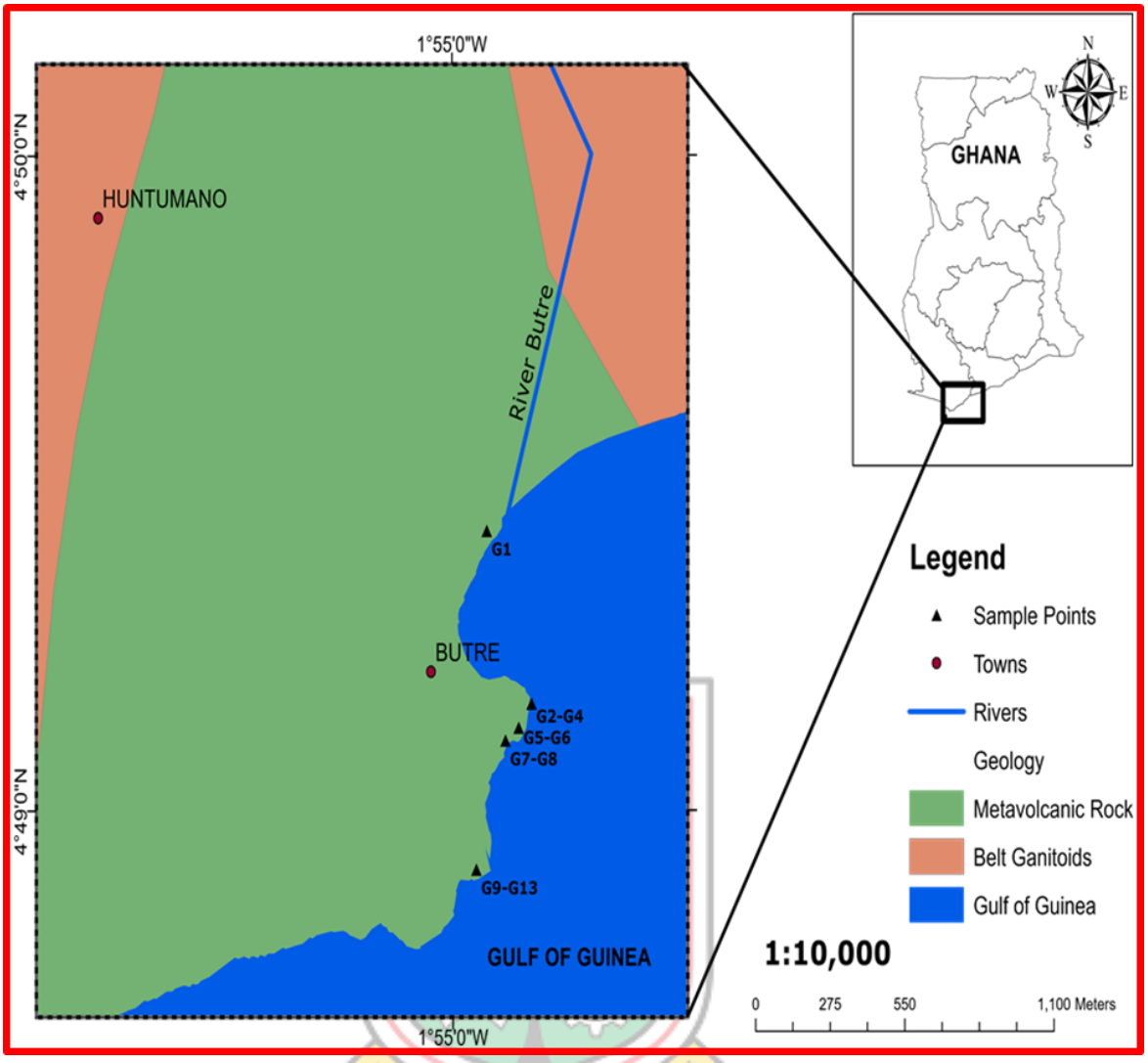


**Figure 3.1 Geological Map of the study Area showing sample locations**

### 3.1.1 Whole Rock Geochemical Analysis

All thirteen (13) representative samples that were studied under the microscopy were selected for whole rock geochemical analysis at the Associated Laboratory Services (ALS) Minerals, Canada, following standard procedures.

Each sample was weighed, crushed using mechanical crusher to about 70 % below 2 mm and splitted using the riffle splitter. It was then pulverised using the agate mortar to about 85 % and made to pass through <75 µm to obtain powdered samples. From each powdered sample, glass discs were prepared using lithium borate flux composed of 50 % lithium tetraborate ($Li_2B_2O_7$) and lithium borate ($LiBO_2$). 0.9 g of ignited powdered samples were added to 9.0 g of lithium borate flux, mixed well and fused in an auto fluxer at about 1100 $^oC$. From the molten melt, a flat glass was prepared and analysed by X-ray fluorescence

spectroscopy for major oxides using the XRF-06 equipment, the upper and lower limits being 100 % and 0.01 % respectively.

For trace elements analysis, 0.2 g of each samples were digested using perchloric (HCLO4), nitric (HNO3), hydrofluoric (HF) and hydrochloric (HCL) acids. The resultant constituents were topped up with dilute hydrochloric acid and analysed for trace elements using inductively coupled plasma atomic emission spectroscopy, correcting spectral inter-element interferences. The authenticity of the analytical procedure (from accuracy to standards) is obtainable at Associated Laboratory Services Minerals, Canada (alsglobal.com).

# CHAPTER 4

## RESULTS

### 4.1 Petrographical Studies

#### 4.1.1 Basalt

In the field, the rock is light green melanocratic, fine to medium grained with mafic minerals although, a sample (G12) had its plagioclase being porphyritic with quartz veins containing sulphides. The host rock occurs in the field as pillow lava (samples G1 and G11) (Figs. 4.1 and 4.2c). It is also massive cut by an intrusive (sample G5) (Fig. 4.2a), as irregularly fractured (samples G9) (Figs. 4.2b) and as sheared (sample G12) cut by sheared quartzo-feldspathic dyke (Fig. 4.2d).

Primary plagioclase is fine grained, subhedral to anhedral, occur in the matrix in association with fine grained amphibole (Amp 1) and show irregular alignment although some moderate alignment was observed (Figs. 4.3f and c). The primary plagioclase rarely shows albite twinning (extinction angle of $95^0$) strongly altered to sericite (which gives a sheen cyan green to light blue colour) and overprinted by aligned amphibole (Amp 2?) that is prismatic and strongly pleochroic from pale yellowish-green to yellowish-green (Fig. 4.3a). Primary plagioclase also is medium grained, euhedral to sub-euhedral, moderately aligned and occur with fine to medium grained amphibole. The plagioclase shows white mineral in the matrix which probably could be carbonate (Fig. 4.3c). These textures of the plagioclase may be related to flow structure. Plagioclase also occur at the hinge and core zones of a fold. It is medium grained, sheared, shows albite twinning at extinction angle of $37^0$ and $34^0$ (all of Andesine composition) and also show weak alteration to fine sericite and quartz (Fig 4.3d). Plagioclase veins that show strong alteration to quartz cut across fine grained matrix of irregularly aligned plagioclase and amphibole. The plagioclase veins are overprinted by opaque minerals (Figs. 4.4a and b).

**Figure 4.1 Photograph of host rock at Butre area showing Pillow structure.**

Amphibole is medium grained, subhedral to anhedral and appears bent (oriented?). It shows strong pleochroism from yellowish green to green, with parallel cleavage at an extinction angle of $7^0$. Amphibole is partially replaced by fine chlorite and pyroxene (Fig. 4.3b). Amphibole 3 is medium grained, anhedral to sub-rounded and appears colloidal. It shows parallel cleavages and pleochroic from pale yellowish green to green (Figs. 4.4c and 4.3e).

Pyroxene is medium grained, subhedral prismatic and granular with characteristic cleavages that are pleochroic from pale green to yellowish-green. It has straight extinction, shows pink alterations and partially corroded by plagioclase (Fig. 4.3d). Pyroxene is also anhedral prismatic with characteristic cleavages and straight extinction. It is clouded by fine plagioclase (Fig. 4.3e).

Epidote is granular and flaky. It is colourless under plane polarised light but violet to yellowish green interfering colours under crossed nicols. It occurs as alteration minerals of pyroxene and plagioclase.


**Figure 4.2 Photograph of host rock at Butre area showing a) massive structure cut by an intrusive b) fractures c) pillow structure with fractures and d) host rock with vein**

Opaque minerals include arsenopyrite, pyrite, magnetite and haematite. Arsenopyrite is subhedral cubic bearing the shape typical of euhedral pyrite. The colour on the other hand is creamy-white and isotropic. This probably may be pyrite with high arsenic composition and is weakly replaced by fine dark brown lines of magnetite (Fig. 4.3d) (Fig. 4.4d). Arsenopyrite that is isotropic and sub rounded with a pale (dirty) white colour is partially replaced by fine magnetite with fine grains of bright yellow mineral (gold?) (Fig. 4.4e). Pale yellow pyrite that is isotropic, anhedral and porphyroblastic replaces anhedral creamy white and isotropic arsenopyrite. Both pyrite and arsenopyrite show inclusions of magnetite. Arsenopyrite in addition to magnetite, shows haematite replacement as well. Closer to this texture, fine grains of bright yellow coloured pyrite (gold?) occur close to arsenopyrite (Fig. 4.4f). Anhedral pale yellow pyrite has replaced (almost completely) creamy white arsenopyrite (which occur at the grain margins of pyrite). Pyrite shows partial replacement

by magnetite and exsolution of bright yellow mineral (probably pyrite that has assimilated arsenic). Near this texture, creamy white, anhedral and isotropic arsenopyrite is being replaced by pyrite. Pyrite shows weak replacement by dark brown magnetite (Fig. 4.5a).

Pyrite is anhedral, isotropic with dimmed yellow colour and partially replaced by fine dark coloured round to sub rounded magnetite. Magnetite at the grain margin is sub rounded and isotropic with a coffee brown colour (Fig. 4.5b). Pale brassy yellow pyrite that is anhedral, isotropic and appears porphyroblastic is being replaced by dark coloured isotropic magnetite in the mineral body and at a portion of the margin. Magnetite at the margin is in turn, being replaced by greyish white, anhedral and isotropic haematite (Fig. 4.5c). Pyrite is also isotropic, anhedral and pale yellow (with a brassy touch), that is moderately lustrous. It is being replaced by anhedral, isotropic greyish white mineral (haematite?) (Fig. 4.5d). Modal percentages of the minerals of the host rocks are shown in Table 4.1.

**Table 4.1 Modal percentage of Basalt at Butre area**

| Minerals/sample ID | G1 | G5 | G9 | G11 | G12 |
|---|---|---|---|---|---|
| Plagioclase | 35 | 40 | 35 | 42 | 40 |
| Amphibole | 40 | 25 | 40 | 36 | 45 |
| Pyroxene | 10 | - | 5 | 5 | - |
| Chlorite | 5 | 3 | 10 | 5 | 5 |
| Sericite | 3 | 10 | 3 | 5 | 4 |
| Epidote | 5 | 5 | 5 | 3 | - |
| Quartz | Tr | Tr | Tr | 1 | 3 |
| Carbonate | - | 15 | - | - | - |
| Arsenopyrite | 1.5 | 1 | 1.9 | 1 | 0.85 |
| Pyrite | 0.2 | 0.6 | Tr | 1 | 2 |
| Magnetite | 0.3 | 0.4 | 0.1 | 0.2 | 0.1 |
| Haematite | - | - | - | 0.1 | 0.05 |
| **Total** | **100** | **100** | **100** | **100** | **100** |

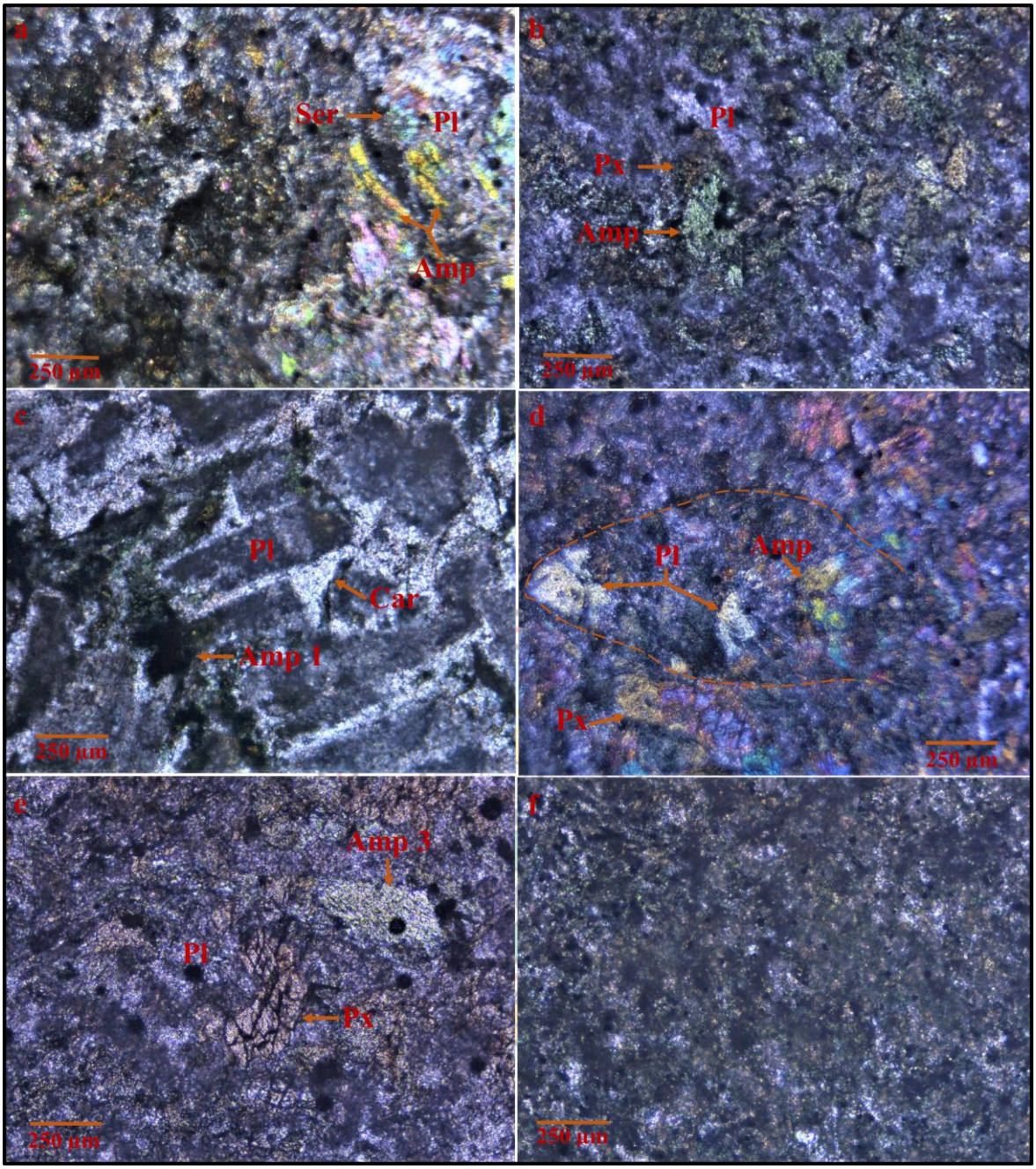


**Figure 4.3 Photomicrograph of Basalt in thin section a) and d) under cross nicols; b), c), e) and f) under plane polarised light.**

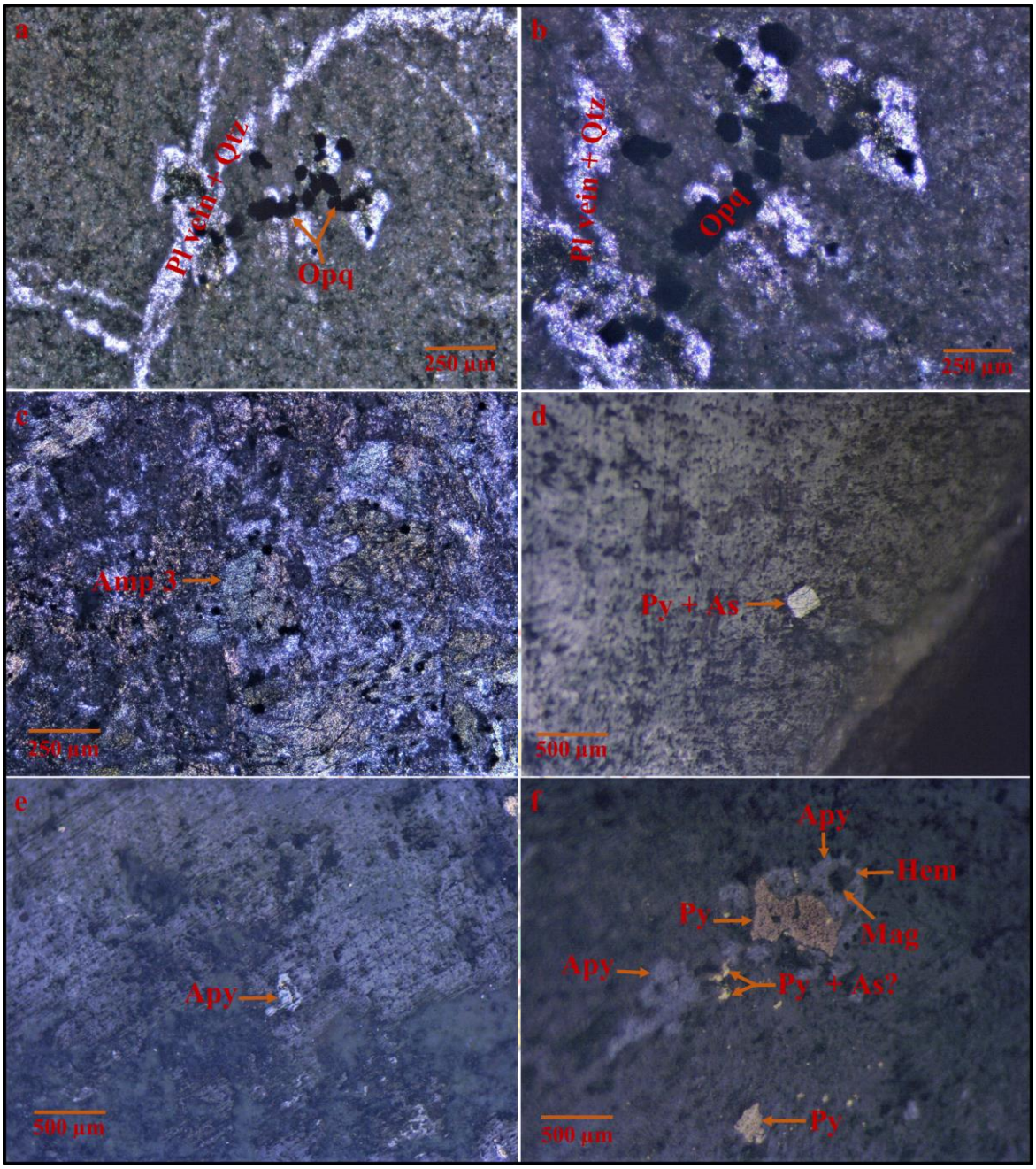


**Figure 4.4 Photomicrograph of Basalt in a) to c) thin section under plane polarised light; d) to f) polished section under reflected light.**

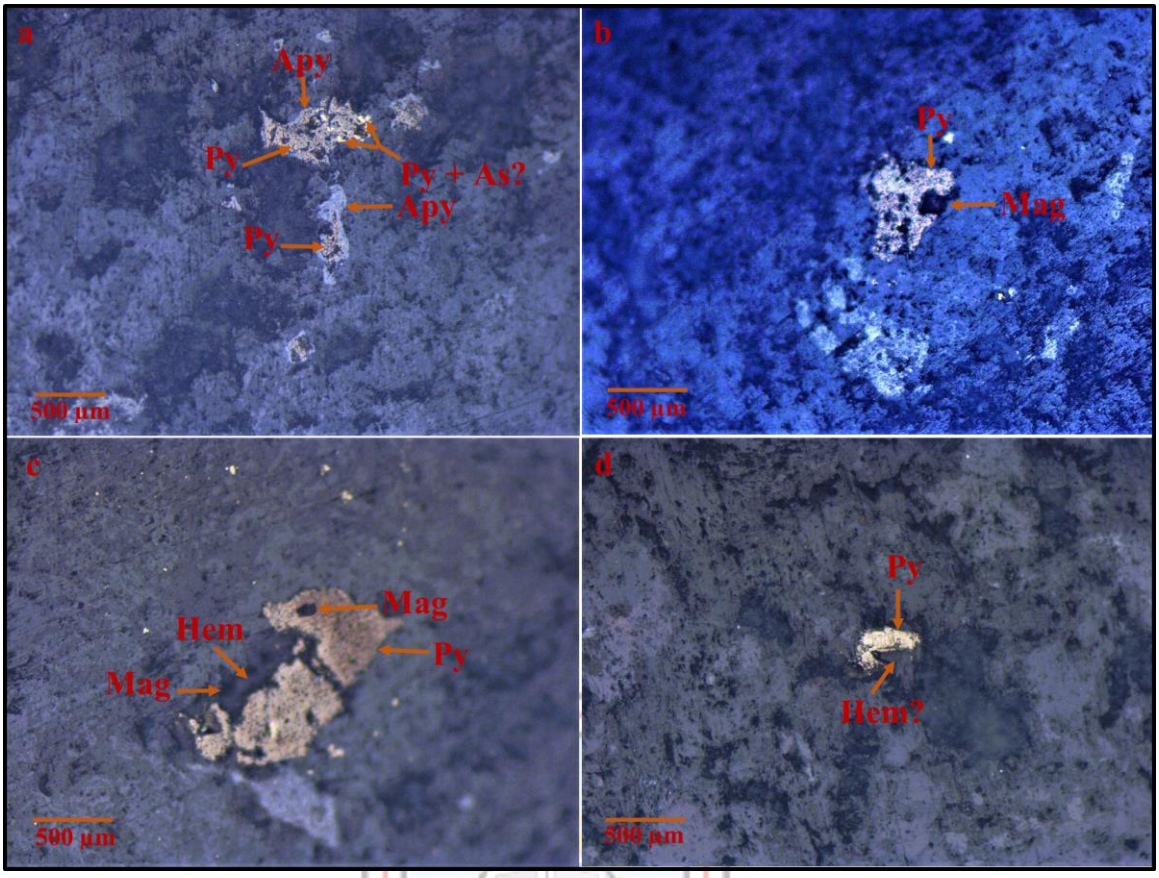


**Figure 4.5 Photomicrograph of Basalt in a) to d) polished section under reflected light.**

### 4.1.2 Diorite

In the field, diorite is light green leucocratic to melanocratic, medium to coarse grained with visible quartz with some sulphides, micro porphyritic to porphyritic plagioclase and amphiboles. The rock occurs as an intrusive in contact with massive basalt (sample G3) (Fig. 4.2a) which shows chilled margins (sample G4) (Fig. 4.6a). Diorite also occur as a quartzo-feldspathic dyke (sample G10) (Fig. 4.6b) and as veins filling irregular fractures in basalt (samples G8 and G13) (Figs. 4.2b and 4.6c). Diorite also shows cross cutting relationship in which a sheared quartzo-feldspathic dyke (sample G6 represented as diorite 1) is cut by another dyke (sample G7 represented as dioite 2) (Fig. 4.6d). The cross cutting structure suggests a possible two generations of diorite.


**Figure 4.6 Photographs of intrusives at Butre area showing; a) chilled margin b) quartzo-feldspathic dyke c) intrusive occupying fracture in host rock and d) sheared intrusive (1) cut by another intrusive (2).**

In thin section, the rock is fine to medium grained, moderately foliated and appears porphyritic with phenocrysts of carbonates and pyroxenes with irregular alignment of fine to medium grained subhedral amphibole and plagioclase in the matrix. The carbonate phenocryst is altered to sericite and epidote and partially replaced by pyroxene. The

pyroxene is granular with plagioclase inclusions, shows straight extinction with cleavages that is weakly pleochroic from pale green to yellowish green (Fig 4.7a). Pyroxene phenocryst also shows weak replacement by fine dark green chlorite (Fig 4.7b).

Plagioclase is fine grained, subhedral to anhedral, shows moderate to irregular alignment and occurs in the matrix with fine to medium grained amphibole. Medium grained amphibole appears later (amp 2), granular and is being replaced by pyroxene and opaque minerals (Fig. 4.7c). Occasionally, fine grained amphibole is overprinted by opaque minerals (Fig. 4.7d). Plagioclase vein that altered to fine sericite and quartz cuts across fine grained matrix made up of irregularly aligned plagioclase and amphibole. The plagioclase is overprinted by hydrothermal opaque minerals (Fig 4.7e).

Amphibole is fine to medium grained, subhedral to anhedral and irregularly aligned. Earlier version (amp 1) is fine grained, appears bent, strongly pleochroic from pale yellowish green to yellowish green and almost parallel to plagioclase. However, later version (Amp 2) is medium grained granular, moderately elongated with parallel cleavages, pleochroic from yellowish green to green and overprints earlier plagioclase and amphibole (Fig 4.7f). Amphibole 3 (which could be metamorphic) occurs close to a plagioclase vein. Amphibole 3 is granular and sub-rounded with parallel cleavages, pleochroic from yellowish green to green and partially replaced by dark coloured chlorite and fine epidote. The plagioclase vein is strongly altered to quartz and sericite and cuts across a fine to medium grained matrix of amphibole (amp 1) and plagioclase. Amphibole 4 is anhedral, elongated and fractured. It shows strong pleochroism from pale yellowish green to yellowish green. Amphibole 4 appears to have come along with the vein (Fig 4.8a).

A quartzo-feldspathic vein with medium grained plagioclase strongly altered to quartz and fine sericite with coarse grained amphibole that shows strong epidote replacement occurring at the margin of the vein. The vein appears to be replacing a fine to medium grained, irregularly aligned matrix of plagioclase and amphibole. (Fig. 4.8b). The vein may be related to diorite 2 and the fine to medium grained matrix relating to diorite 1 (all in relation to the cross cutting structure observed in the field). A weakly deformed intrusion made up of medium to coarse grained, subhedral and irregularly aligned plagioclase and amphibole that are strongly altered to fine sericite and epidote, respectively, into fine to medium grained matrix of plagioclase and amphibole may suggest a possible two generations of diorite (Fig.

4.8c). A fine grained irregularly aligned plagioclase and amphibole embedded in a medium to coarse grained matrix of strongly altered plagioclase and amphibole may be a microscopic basaltic xenolith caught up in diorite (diorite 1 or 2?). (Fig. 4.8d). A cluster of aligned coarse grained, granular amphibole that is surrounded by fine grained, irregularly aligned amphibole and plagioclase suggest an amphibolite xenolith caught up by the rock. This coarse grained amphibole is overgrown by weathered garnet (Fig.4.8e). A possible magma mixing between diorite 1 and a felsic intrusive has resulted in an anhedral (with the shape of the African map) texture with fine grained, anhedral and irregularly aligned plagioclase (Fig. 4.8f). Epidote gives violet, blue and yellow birefringent colours under crossed nicols but is colourless under plane polarised light and occurs as an alteration products of carbonate, pyroxene and amphibole.

Opaque minerals identified include arsenopyrite, pyrite, magnetite and haematite. Arsenopyrite is creamy white subhedral to anhedral, isotropic, occurs in gangue mineral and weakly corroded by gangue mineral (Fig 4.9a). Subhedral and isotropic arsenopyrite is partially corroded by lighter gangue mineral and partially replaced by pyrite and fine magnetite at the core zone (Fig 4.9b). Pale yellow with brassy touch, anhedral, isotropic pyrite partially replaces by arsenopyrite. Pyrite is in turn being replaced by dark brown magnetite and greyish white haematite (Fig 4.9c). Sub-rounded, isotropic pyrite with a dimmed pale yellow colour forms a rim around arsenopyrite. Arsenopyrite is being replaced by haematite and fine dark brown magnetite which occurs at grain margins of haematite and arsenopyrite at the core. Haematite also occur at the grain margins of pyrite (Fig. 4.9d). A cluster of porphyroblastic, anhedral pyrite shows exsolution of arsenopyrite at grain margins and is partially replaced by dark brown spots of magnetite (Fig. 4.9e). Pyrite also show blurby shape and clouded by fine magnetite (Fig. 4.9f). Modal percentages of the minerals are shown in Table 4.2.

**Table 4.2 Modal percentage of Diorite at Butre area**

| Minerals/ Sample ID | G3 | G4 | G6 | G7 | G8 | G10 | G13 |
|---|---|---|---|---|---|---|---|
| Amphibole | 32 | 25 | 48 | 30 | 46 | 39 | 53 |
| Plagioclase | 27 | 50 | 31 | 42 | 25 | 42 | 27 |
| Pyroxene | 20 | 5 | - | - | 10 | - | - |
| Epidote | 7 | 3 | 5 | 4 | 3 | 2 | 4 |
| Sericite | 5 | 6 | 5 | 5 | 5 | 5 | - |
| Chlorite | 4 | 5 | 5 | 8 | 7 | 5 | 5 |
| Quartz | 3 | 4 | 3 | 6 | 3 | 5 | 2 |
| Tourmaline | - | 0.5 | - | - | - | - | - |
| Actinolite | - | - | 2 | - | - | - | - |
| Apatite | - | - | - | - | - | - | - |
| Garnet | - | - | - | - | - | - | 1 |
| Pyrite | 0.5 | 1 | 0.7 | 3 | 0.7 | 1.7 | 3 |
| Arsenopyrite | 1 | 0.3 | 0.2 | 1.5 | 0.3 | 0.1 | 4 |
| Magnetite | 0.5 | 0.1 | 0.1 | 0.5 | - | 0.2 | 1 |
| Gold | - | 0.1 | - | - | Trace | - | - |
| Haematite | - | - | Trace | - | - | - | - |
| Limonite | - | - | - | - | - | - | 0.05 |
| **Total** | 100 | 100 | 100 | 100 | 100 | 100 | 100 |

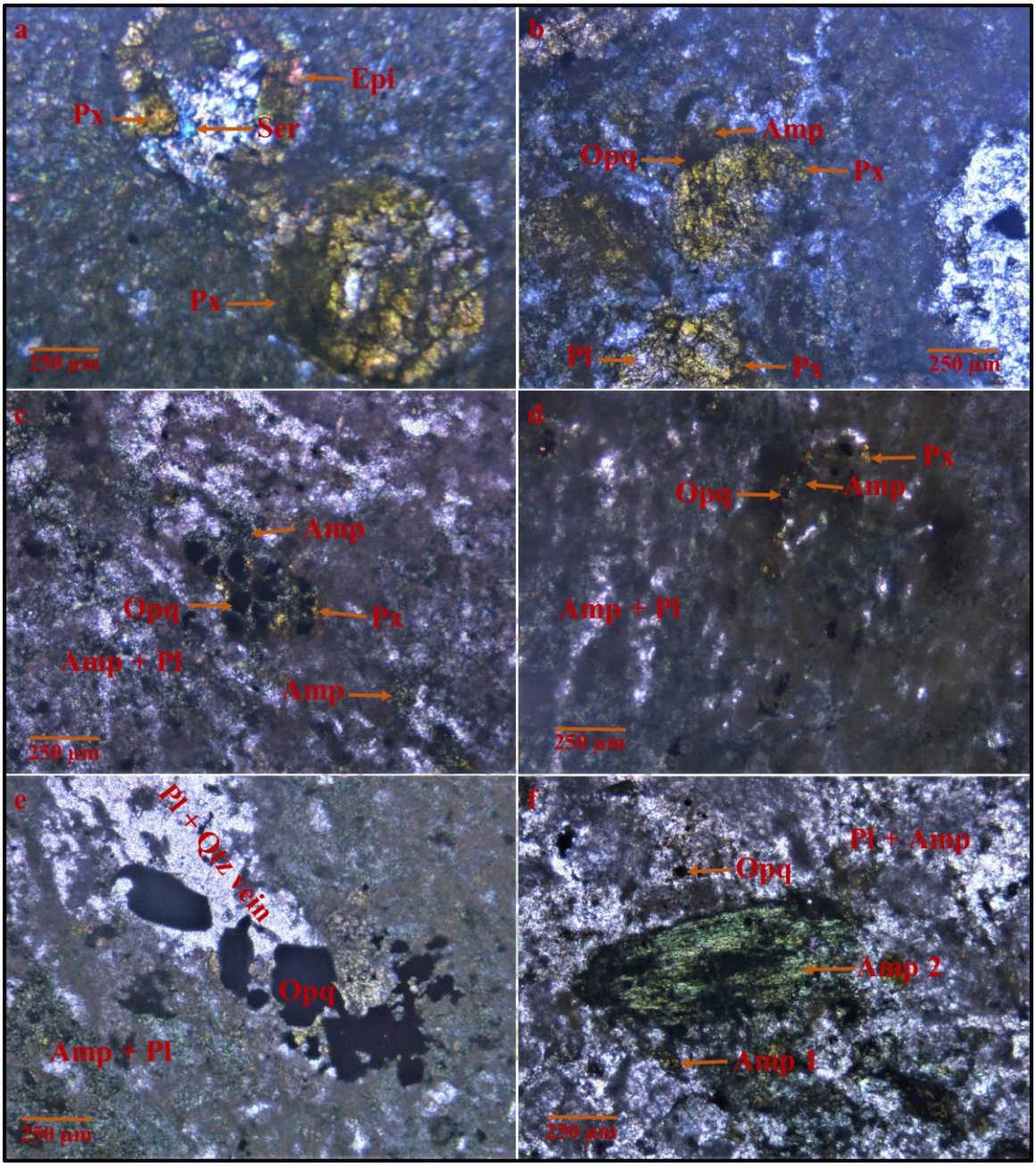


**Figure 4.7 Photomicrograph of Diorite in Thin Section a) to f) under plane polarised light.**

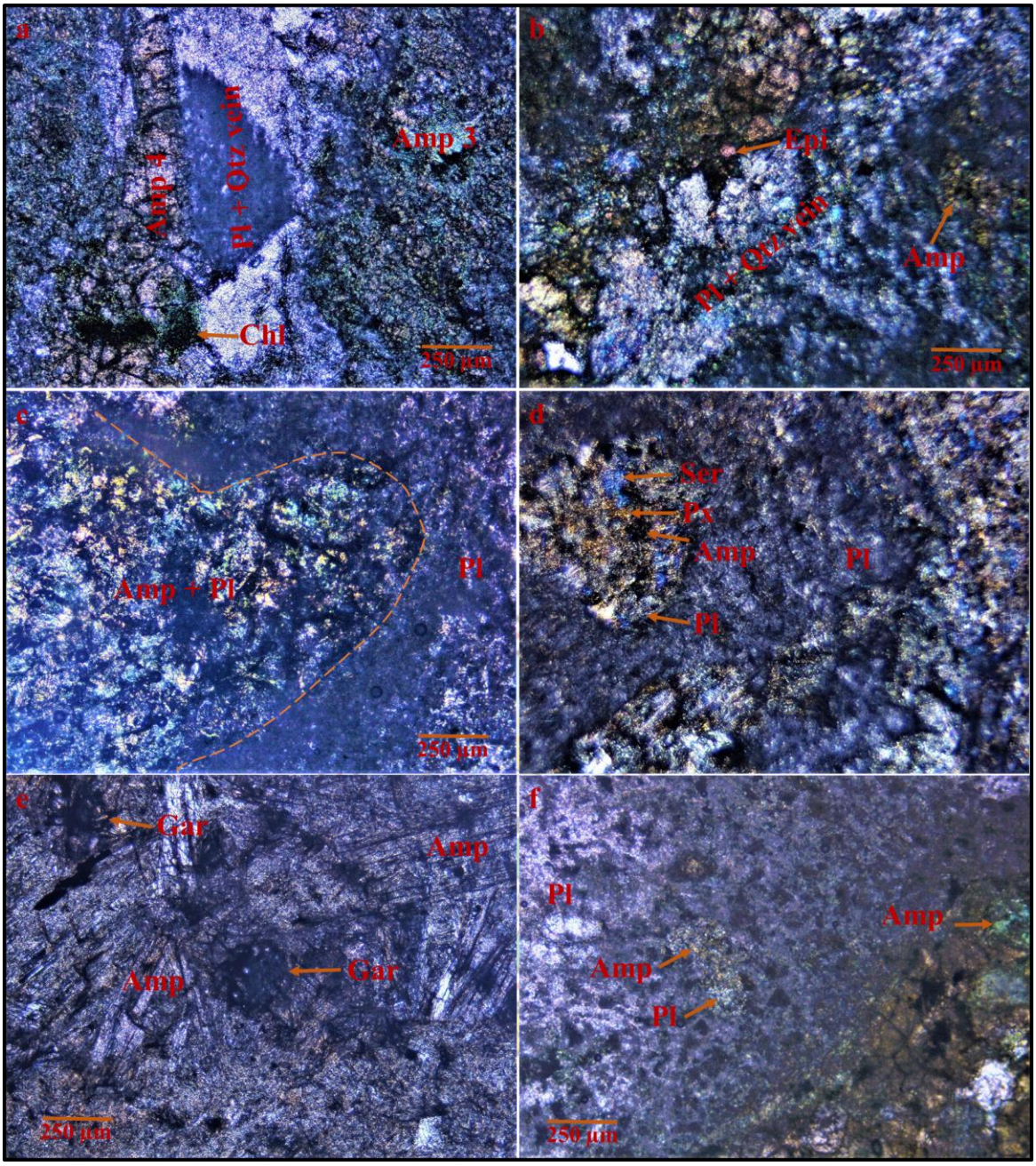


**Figure 4.8 Photomicrograph of Diorite in Thin Section a) and b) cross nicols; c) to f) under plane polarised light.**

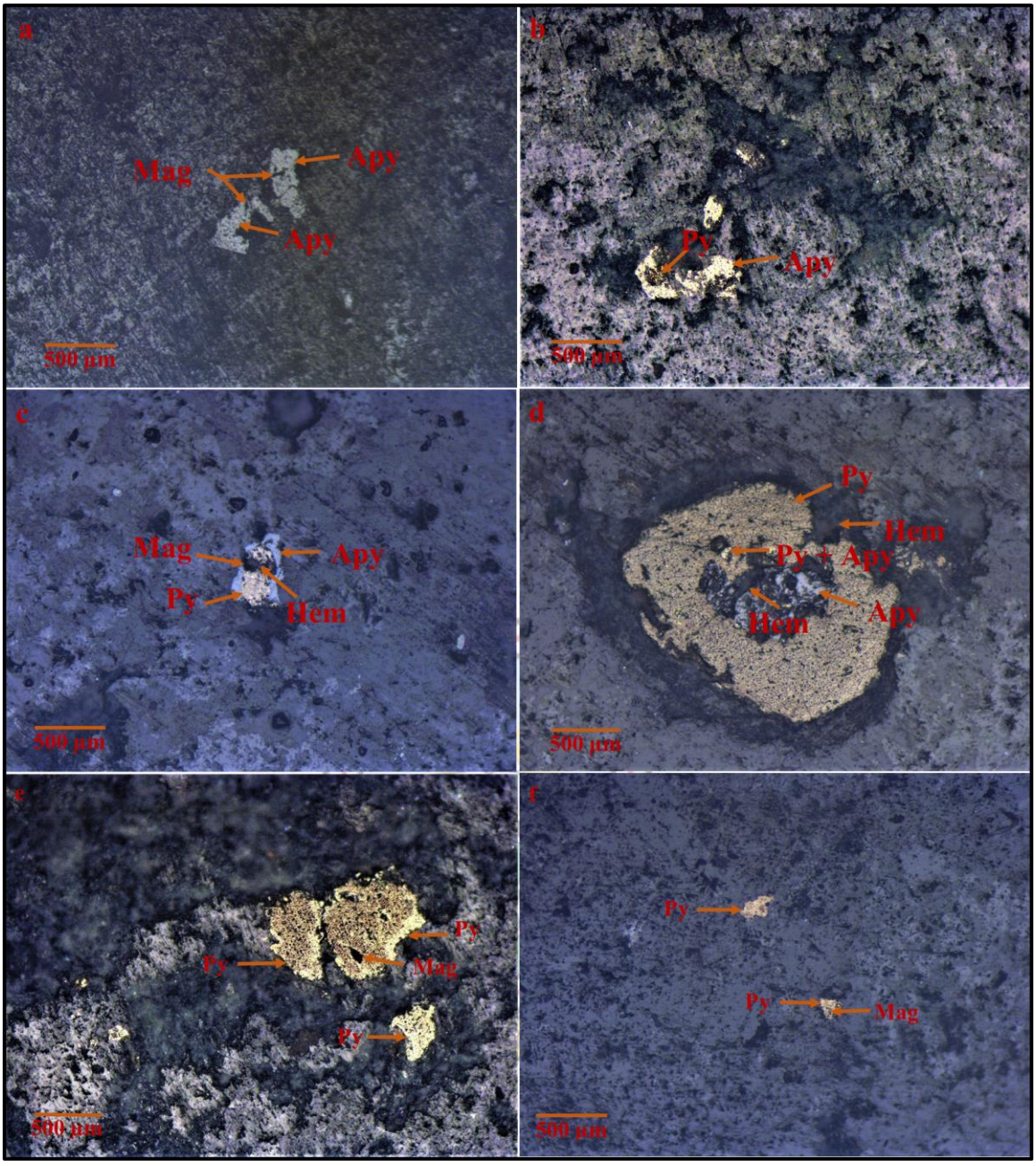


**Figure 4.9 Photomicrograph of Diorite in Polished Section a) to f) under reflected light**

### 4.1.3 Granodiorite

In the field, granodiorite is light green leucocratic, coarse grained with visible quartz, sulphides, porphyritic plagioclase and amphiboles. Rock occurs as a quartzo-feldspathic veins (sample G14) filling fractures in basalt (host rock with high quartz content) (Fig. 4.2d). In thin section, granodiorite is medium to coarse grained with moderate alignment of subhedral plagioclase and amphibole. Earlier fabric shows moderately aligned textures

made up of fine to medium grained plagioclase and amphibole (amp 1). Plagioclase is strongly altered to quartz and fine sericite. Amphibole is weakly altered to fine chlorite (Figs. 4.10a and b). The earlier fabric is overprinted by later amphibole (amp 2). Amphibole 2 is coarse grained, granular and cuts foliation. It is fractured with parallel cleavages, pleochroic from pale yellowish green to green. It is partially altered to fine chlorite (Figs. 4.10b and c). Opaque minerals include anhedral, isotropic pale yellow pyrite that is partially replaced by a purple, light blue and green mixed coloured mineral (pyrhotite?). (Fig 4.10d).

*Summary of Thin and Polished Section of Intrusives*

The rocks show medium to coarse grained textures with moderate to irregular alignment of minerals. A cross cutting structure observed in the field suggests a possible two generations of diorite which were represented as diorite 1 and 2. A sheared coarse grained porphyritic rock (quartz diorite) was differentiated from the more similar diorite. Although the diorites show similar mineralogy, diorite 1 has more amphibole composition than diorite 2. Plagioclase (as compared to amphibole) composition is higher in diorite 2 than diorite 1. Pyroxene composition is high in diorite 2 than diorite 1, which strongly to weakly replaces amphibole in diorite 2 than diorite 1. Quartz content is also higher in diorite 2 than diorite 1. Generally, plagioclase shows weak to strong alteration to sericite and quartz; amphibole to chlorite and epidote with replacement by pyroxene; pyroxene to chlorite and epidote. Opaque minerals are pyrite and arsenopyrite that shows weak replacement by magnetite and haematite. Diorite 1 shares similar opaque mineral variations with the host rock, in that, arsenopyrite is being replaced by pyrite. Diorite 2 on the other hand is more pyrite mineralised. Modal percentages are given in Table 4.3.

**Table 4.3 Modal percentage of Granodiorite at Butre area**

| | **Sample ID** |
|---|---|
| Mineral | **G14** |
| Amphibole | 25 |
| Plagioclase | 50 |
| Quartz | 13 |
| Sericite | 5 |
| Chlorite | 2 |
| Apatite | 2 |
| Epidote | 1 |
| Pyrite | 1 |
| Magnetite | 0.5 |
| Pyrrhotite | 0.1 |
| Tourmaline | 0.4 |
| **Total** | 100 |

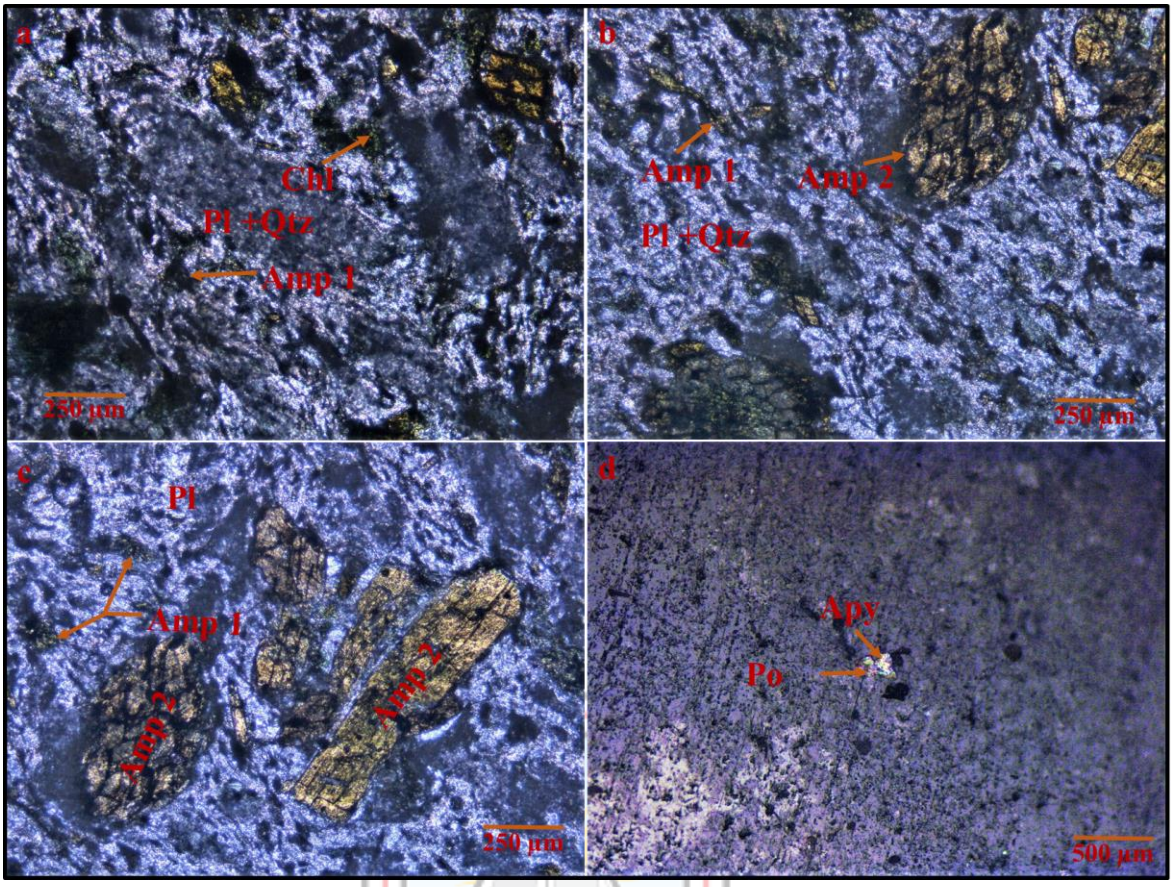


**Figure 4.10 Photomicrograph of Granodiorite in a) to c) Thin Section under Plane Polarised Light; d) Polished Section under reflected lightight**

## 4.2 Whole Rock Geochemistry

All thirteen (13) representative samples were analysed at Associated Laboratory Services Minerals, Canada using X-ray fluorescence and ICP-ES. Result of the analysis is given in Appendix 1.

NB: definitive conclusions were not drawn from petrographical studies to differentiate the intrusives as they bear similar mineralogy. Although evidence of two generations of diorite (from the field and petrography) occur in the study area, geochemical plots were used to classify these rocks.

From whole rock geochemical analysis, silica content of host rock ranges from (47.7 – 61.9 wt.%), which are grouped into two categories namely, lower silica variety (four samples) and silica rich variety (one sample), respectively. The lower silica rich variety (samples G1, G5, G9 and G11) has silica content of (47.7 – 52.6 wt.%) and high silica variety (G12),

(61.9 wt.%). The silica content of the intrusives ranges from (52.6 – 62.7 wt.%) for diorite and (65 wt.%) for quartz diorite. Like the host rocks, diorite is grouped according to their silica content as low and high silica varieties, respectively. The low silica variety ranges from (52.6 – 56.6) $SiO_2$ wt.% and (58.3 – 62.7 wt.%) for the high silica variety type. Generally, all rock types show a fairly and almost constant $Al_2O_3$ content from (11.10 – 15.45 wt.%). The host rock recorded the highest $FeO_T$ (5.56 – 13.35 wt. %) with the high silica diorite (9.49 -11.25 wt. %) but generally low to intermediate in the high silica diorite (5.56 - 9.28 wt.%). The host rock and the low silica diorite also, show high CaO content from (4.96 – 13.65 wt.%) and (8.29 – 15.35 wt.%), respectively, but the high silica diorite shows low CaO content with a range of (3.03 – 6.95 wt.%). MgO content is highest in host rock (2.68 – 10.15 wt.%) and similar in both types of diorite with ranges (2.21 – 7.5 wt.%) for low silica diorite and (2.87 – 7.38 wt.%) for high silica diorite, respectively. The low silica diorite had the lowest $Na_2O$ content (0.13 – 1.94 wt. %). However, the host rock and the high silica diorite had intermediate amounts ranging from (1.35 – 4.46 wt. %) and (2.78 – 4.11 wt. %), respectively. Comparing the elements Hf, Nb, Th and Zr, Hf is enriched in high silica diorite with a range of (1.5 – 3 ppm), intermediate in host rock (1.2 – 2.2 ppm) and low in low silica diorite (0.8 – 1.8 ppm). Nb is enriched in host rock (1.5 – 5.9 ppm) but intermediate in the diorite with ranges (2.2 – 3.3 ppm) for high silica diorite and (1.6 – 2.6 ppm), respectively. Th is least in low silica diorite (0.17 – 0.65 ppm), low to intermediate in host rock (0.2 – 1.9 ppm) and highest in high silica diorite (0.67 – 4.16 ppm). For Zr, the high silica diorite recorded the highest (60 – 109 ppm), followed by the host rock (42 – 81 ppm) with the low silica diorite recording the least (35 – 67 ppm).

Line graphs of some major oxides and trace elements are plotted against each other to classify the host rock and intrusives (Figs 4.14 and 4.15). Discriminatory diagrams to show the tholeiitic and calc-alkaline trends of the various rocks are also given in (Fig 4.14 and 4.15). Binary plots of some major oxides against $SiO_2$ wt. % show the various distribution trends of these oxides in the various rocks (Figs 4.16 and 4.17b and c). The AFM ternary diagram (Fig. 4.17a) shows the two magma series for the rocks from Butre area: tholeiitic and calc-alkaline series. Chondrite normalised REE patterns are illustrated in Fig. 4.19a. The possible tectonic environments of the rocks from Butre area are shown in Figs. 4.17 and 4.18. The possible magma sources of the intrusives at Butre area are also illustrated in Fig. 4.19b.

### 4.2.1 Alteration Box

The alteration box seeks to represent graphically alteration captured under two main indices; the Ishikawa alteration index (AI) and the chlrorite-carbonate-pyrite index (CCPI). The Ishikawa alteration index is given by $\text{AI} = \frac{100(K_2O+MgO)}{CaO+MgO+K_2O+Na_2O}$ (1)

This index is useful in the determination of the extent of sericite and chlorite alteration defined by Ishikawa *et al*. (1976). The index is governed by two reactions;

The replacement of sodium (Na) in albite by potassium (K) in the formation of sericite (Eastoe *et al.,* 1987) and

The replacement of potassium (K) in sericite by magnesium (Mg) and iron (Fe) to form chlorite (Schardt *et al*., 2001).

The CCPI was formulated by (Large *et al*., 2001) to cater for two main limitations of the AI;

- The AI does not consider carbonate alterations which usually lead to lower values in AI although the intensity of alteration is high and
- The AI does not discriminate between sericite and chlorite alterations when used alone.

The chlorite-carbonate-pyrite index is given by $\text{CCPI} = \frac{100\ (MgO+FeO)}{(MgO+FeO+\ Na_2O+K_2O)}$ (2).

Hence the index quantifies the increase in MgO and total FeO ($FeO+Fe_2O_3$) linked to Mg-Fe chlorite formation. An advantage of this index is that, it is sensitive to Mg-Fe carbonate alteration and magnetite and haematite enrichment. Generally, a loss in $K_2O$ with substantial increase in FeO and MgO favours chlorite alteration with the condition that $Al_2O_3$ remains constant. Since the rocks from the study area are igneous rocks, the alteration indices were used to investigate some alteration packages these rocks possess. Various alteration box plots are given in Figs 4.20.

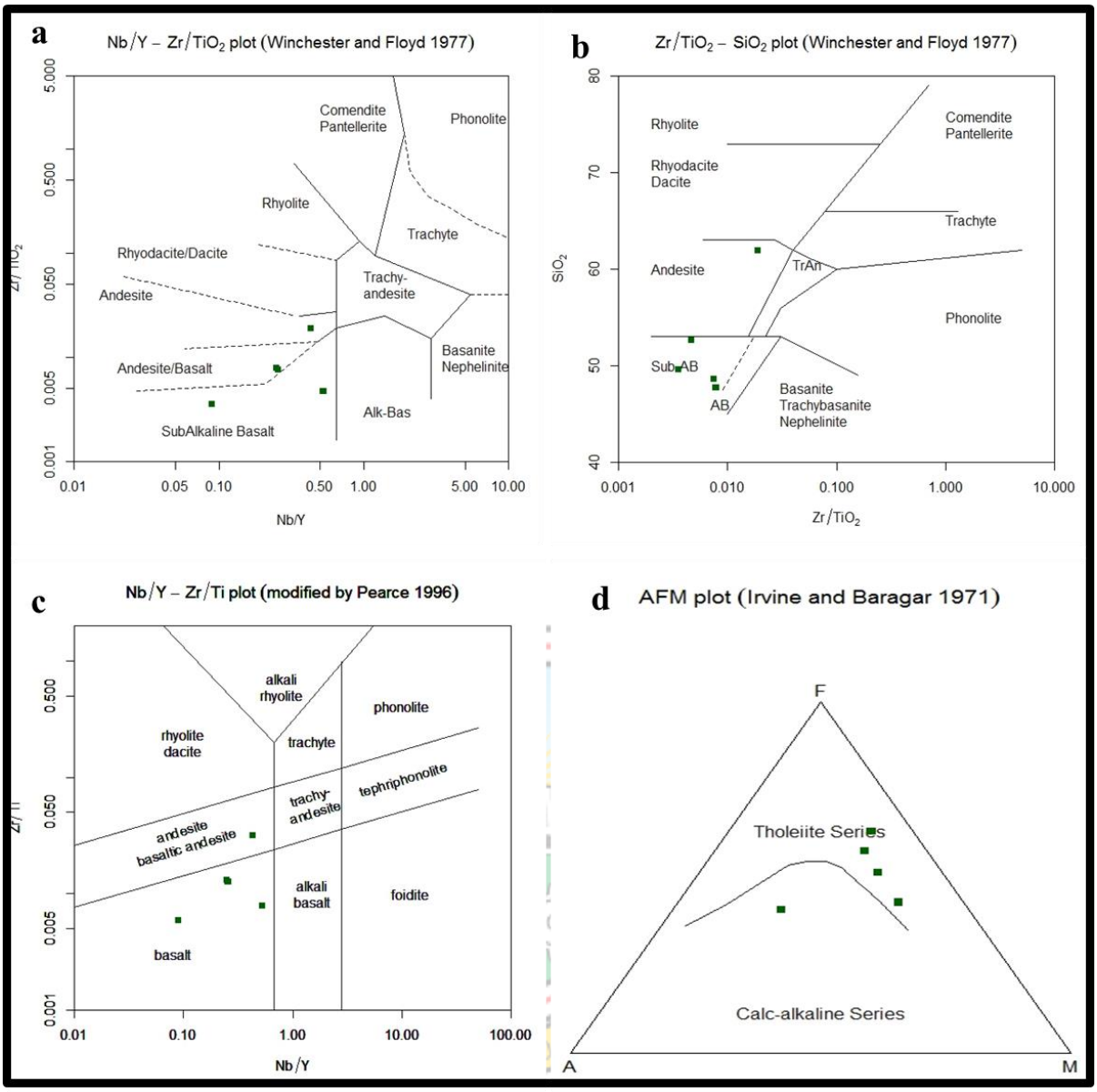


**Figure 4.11 Classification diagrams of Volcanic rocks from Butre Area showing a) Nb/Y against $Zr/TiO_2$ (after Winchester and Floyd, 1977); b) $Zr/TiO_2$ against $SiO_2$ (after Winchester and Floyd, 1977); c) Nb/Y against Zr/Ti (after Pearce, 1996) and d) AFM diagram (after Irvine and Baragar, 1971)**

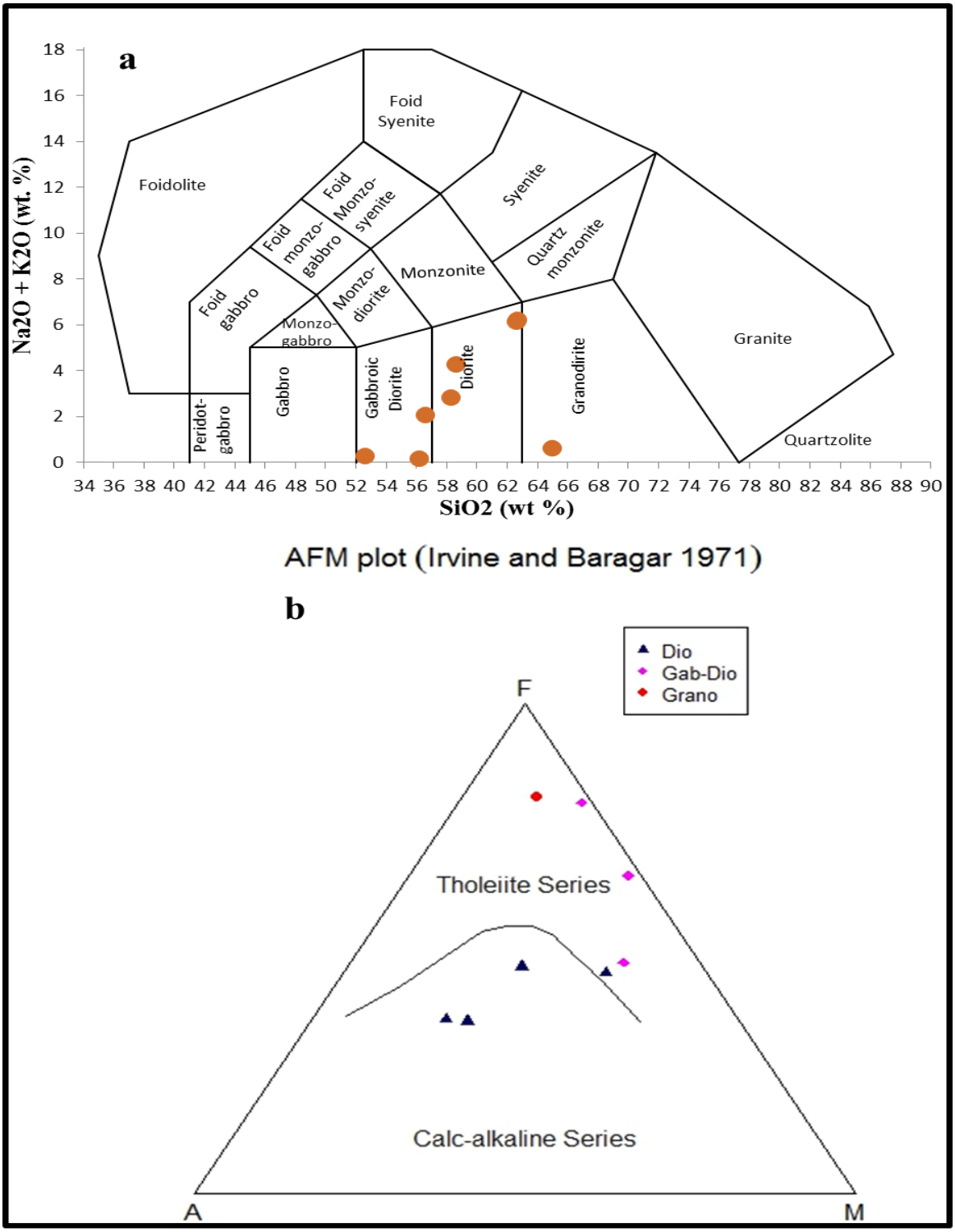


**Figure 4.12 Classification diagrams of plutonic from Butre Area showing a) $Na_2O$ + $K_2O$ against SiO2 (after Middlemost and b) AFM diagram (after Irvin and Baragar, 1971)**

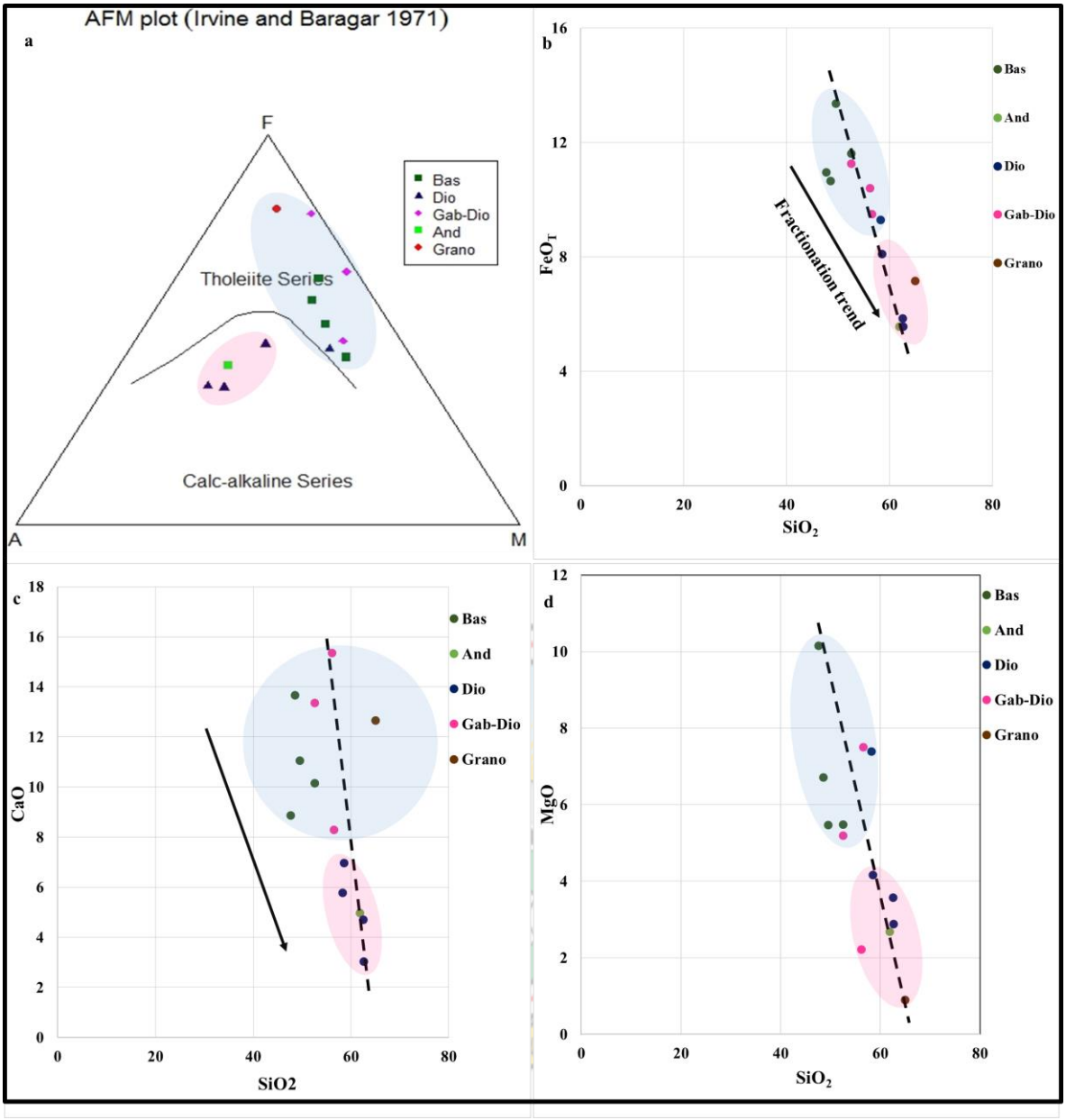


**Figure 4.13 Ternary and Binary Geochemical Plots showing a) AFM diagram of Rocks (after Irvine and Barager, 1971); b) $FeO_T$ against $SiO_2$; c) CaO against $SiO_2$ and d) MgO against $SiO_2$**

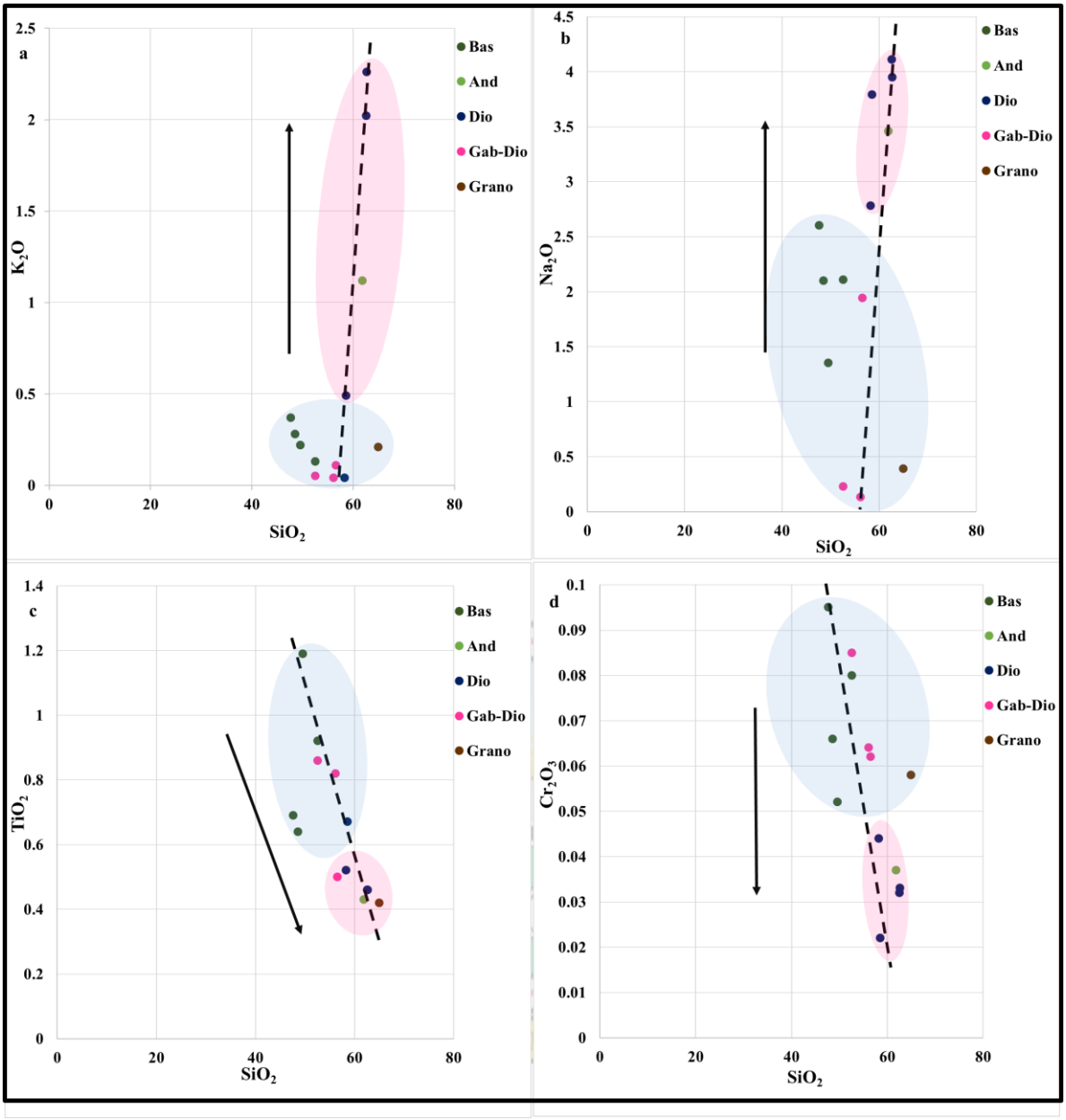


**Figure 4.14 Binary Geochemical Plots of Rocks from Butre Area showing a) $K_2O$ against $SiO_2$; b) $Na_2O$ against $SiO_2$; c) $TiO_2$ against $SiO_2$ and d) $Cr_2O_3$ against $SiO_2$**

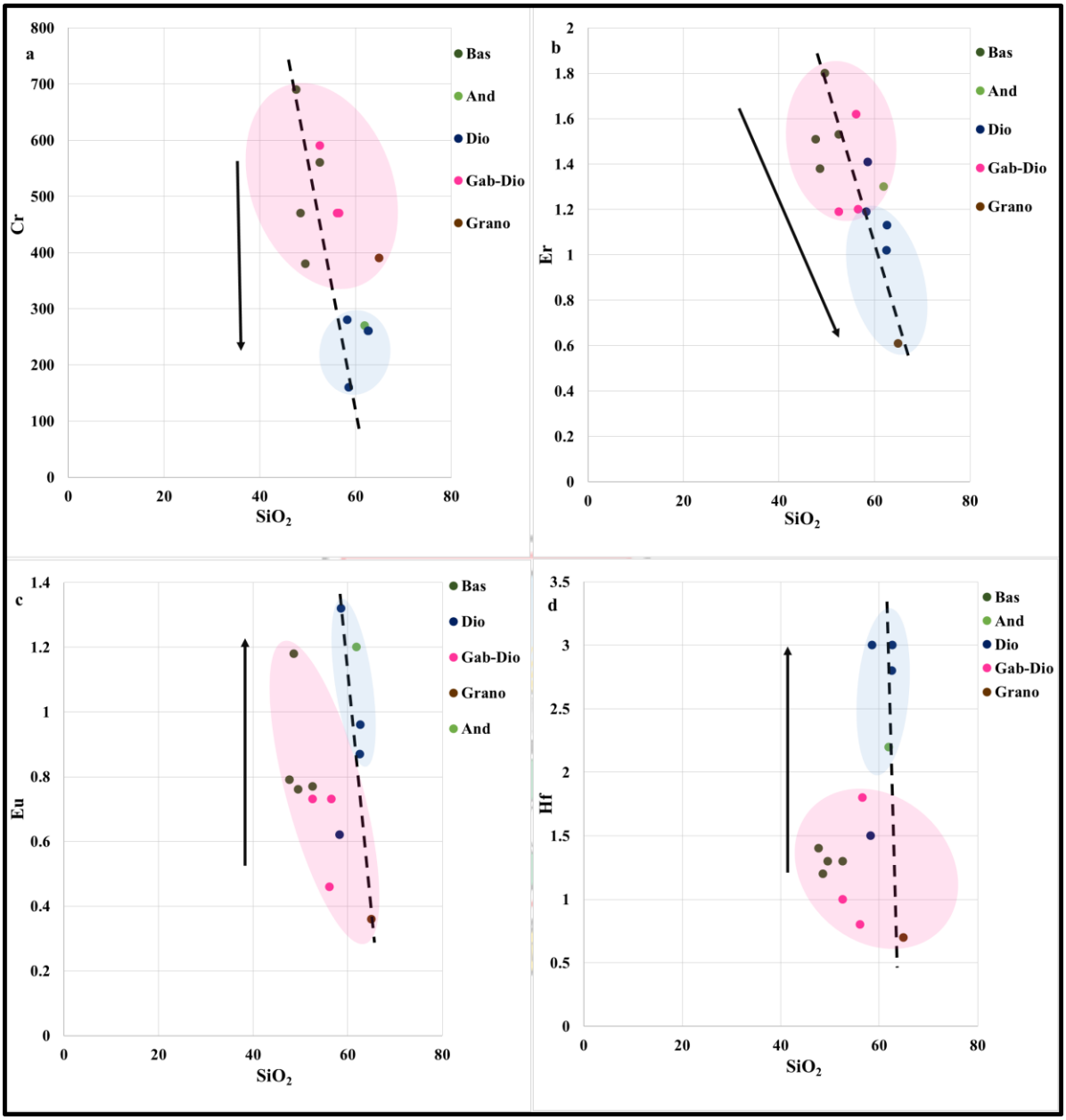


**Figure 4.15 Binary Geochemical Plots of Rocks from Butre Area showing a) Cr against $SiO_2$; b) Er against $SiO_2$; c) Eu against $SiO_2$ and d) Hf against $SiO_2$**

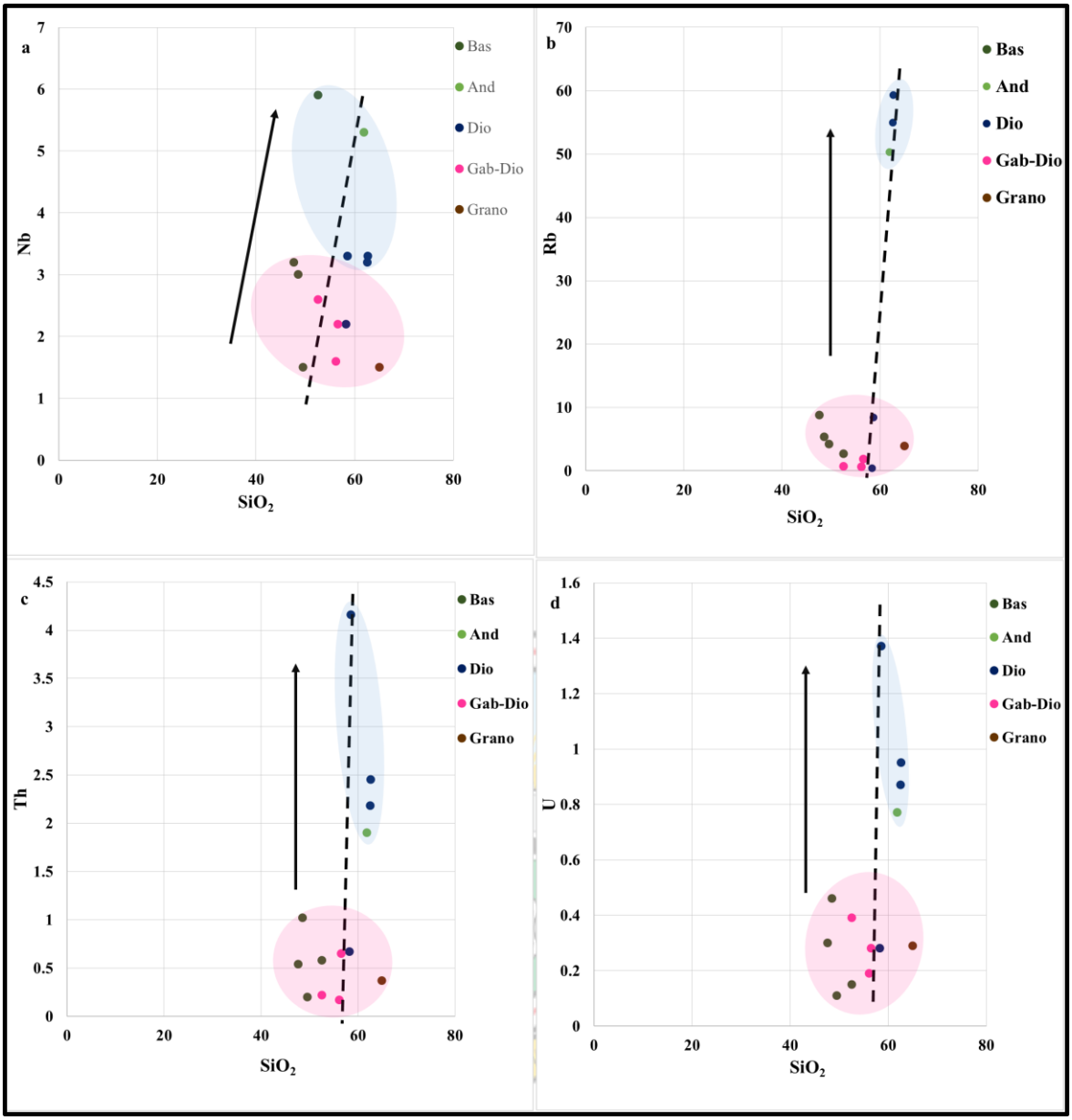


**Figure 4.16 Binary Geochemical Plots of Rocks from Butre Area showing a) Nb against $SiO_2$; b) Rh against $SiO_2$; c) Th against $SiO_2$ and d) U against $SiO_2$**

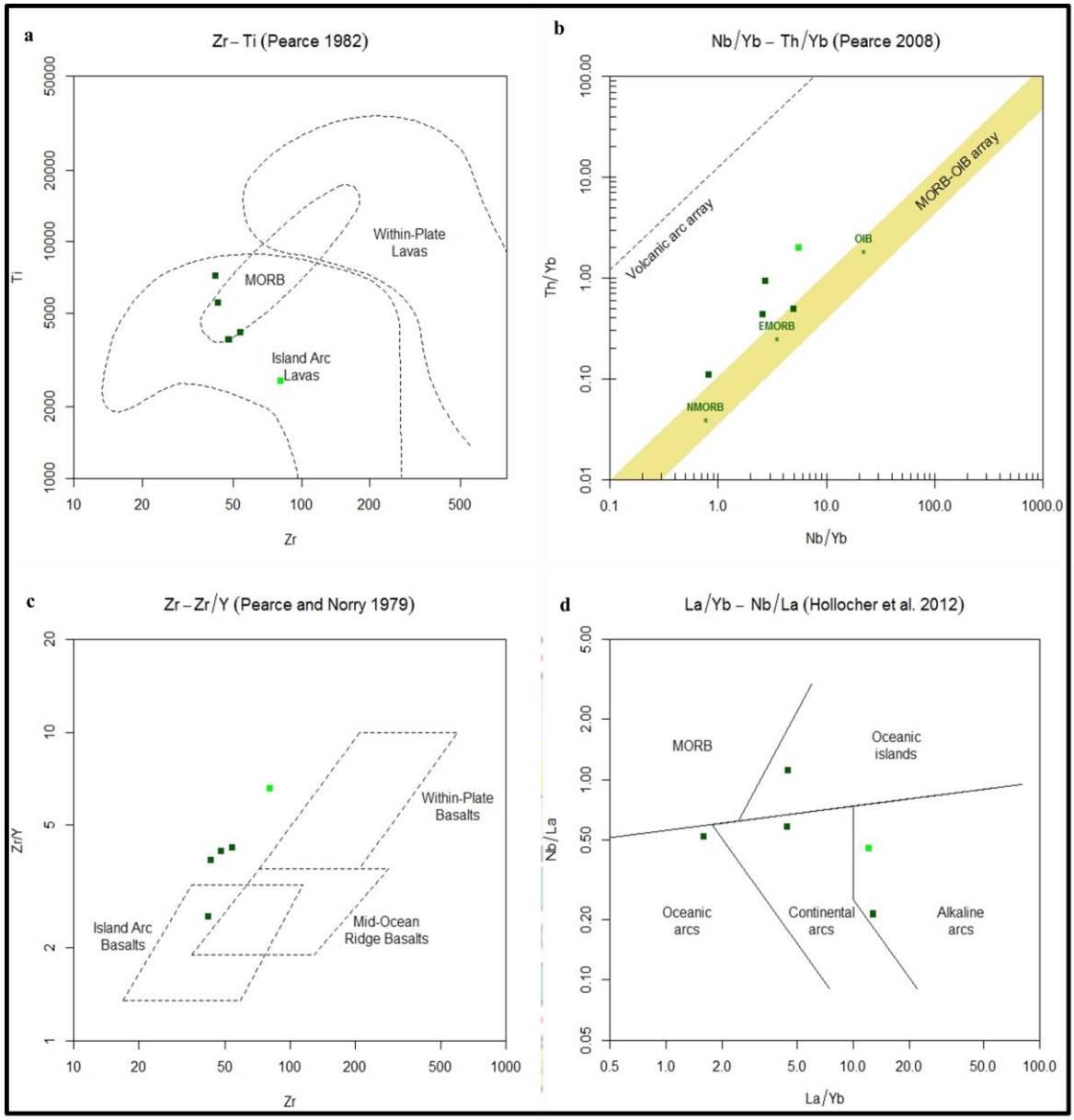


**Figure 4.17 Ternary Plots of Tectonic Settings of Host Rock from Butre Area showing a) Zr-Ti (after Pearce, 1982); b) Nb/Yb-Th/Yb (after Pearce, 2008); c) Zr-Zr/Y (after Pearce and Norry, 1979) and d) La/Yb-Nb/La (after Hollocher *et al.*, 2012).**

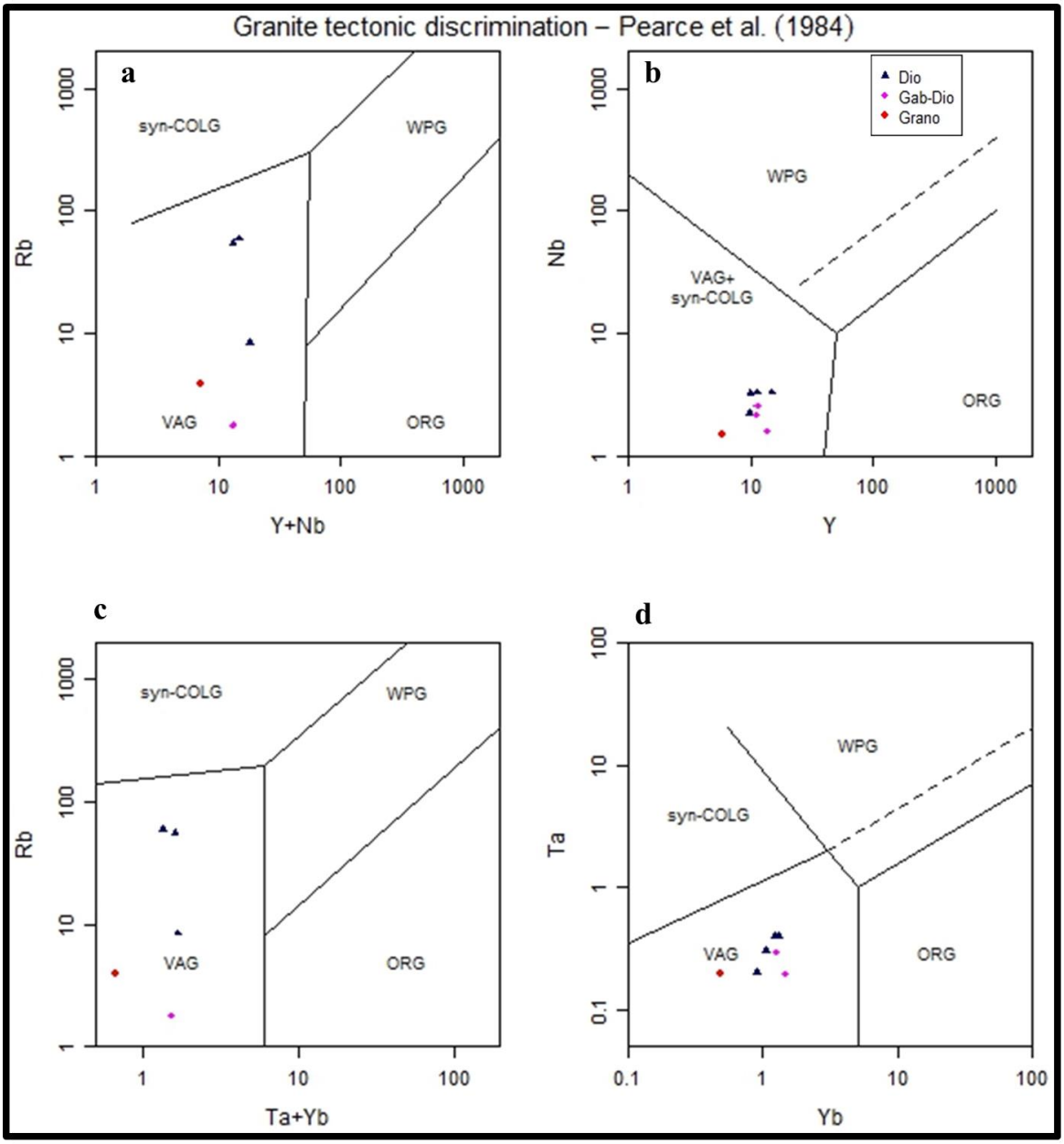


**Figure 4.18 Binary Plots Showing Tectonic Settings of Intrusive Rocks from Butre Area (after Pearce *et al.*, 1984).**

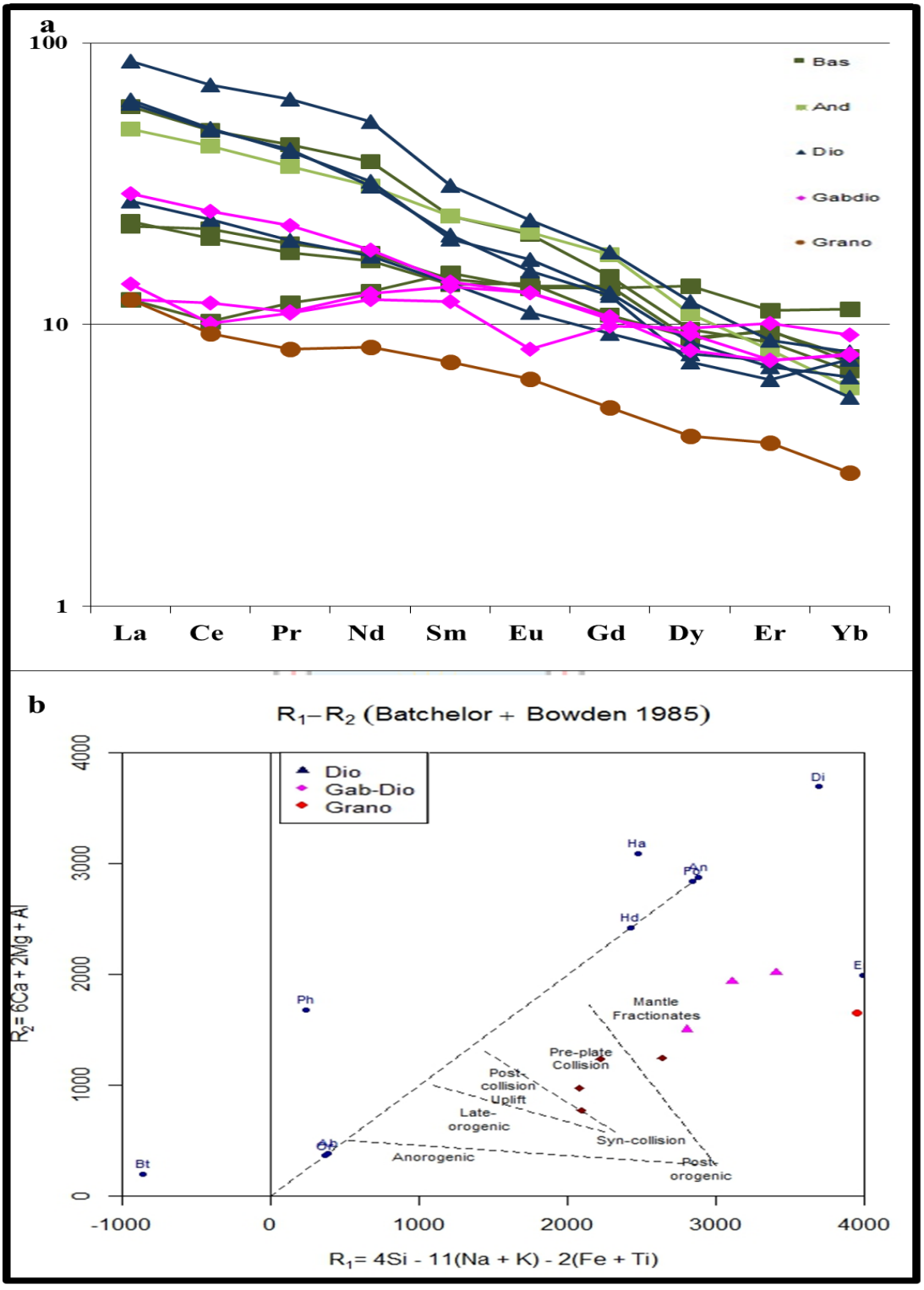


**Figure 4.19 Spider and Binary plot showing a) Chondrite Nomalised REE Patterns of Rocks (Chondrite Normalisation Factors after Sun & McDonough, 1989) and b) Magma Sources of Intrusive Rocks from Butre Area (after Batchelor and Bowden, 1985).**

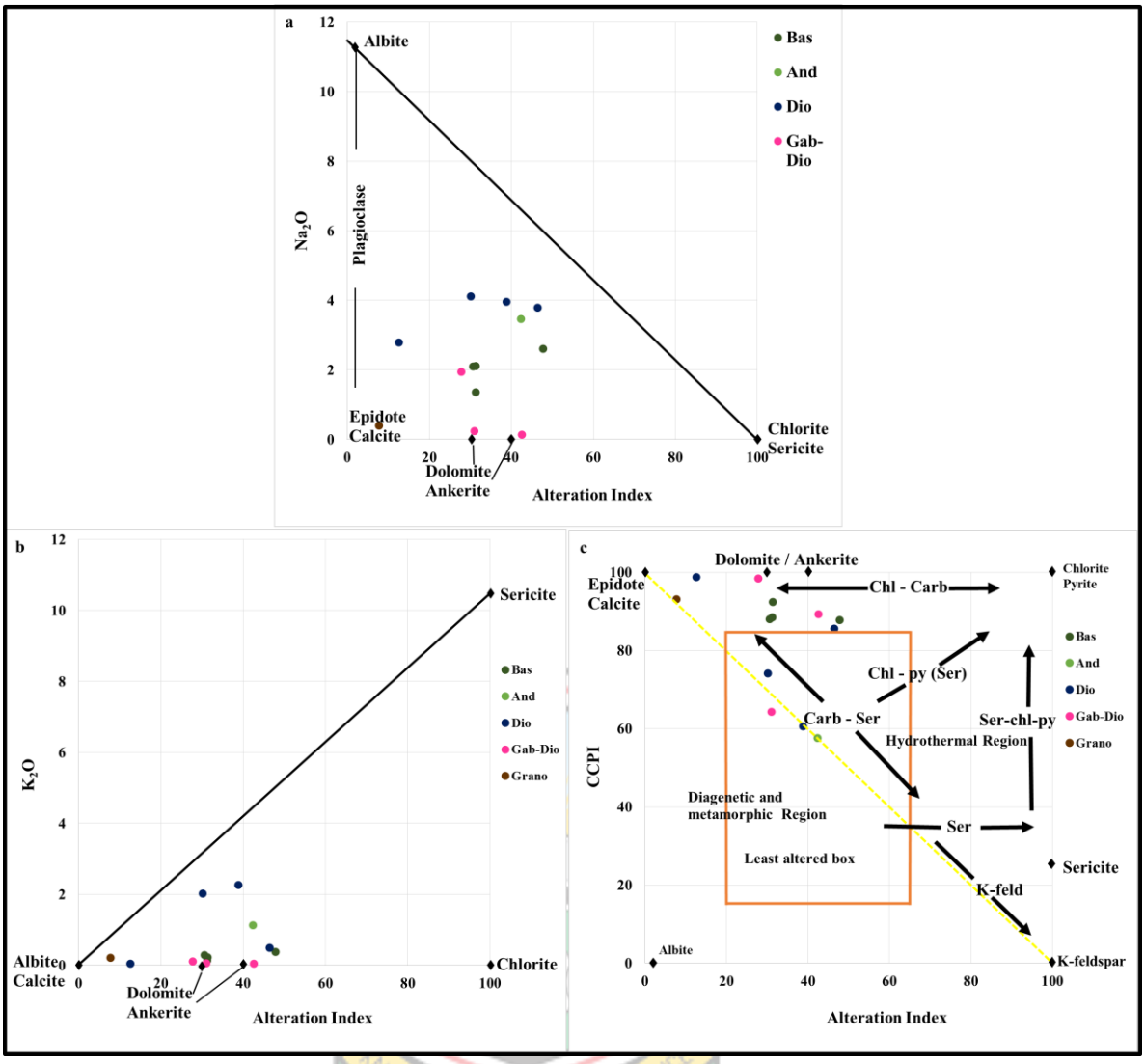


**Figure 4.20 Alteration Box Diagrams Showing Trends of Ishikawa Alteration Index (AI) against a) Na2O wt.% b) K2O wt.% and c) CCP index**

# CHAPTER 5

## DISCUSSION

The major rocks in the study area are basalt and andesite (Fig. 4.11a and b) which are medium grained, massive, fractured with deformed pillow structures (Fig. 4.1 a-d). According to Sylvester and Attoh, (1992), pillows and massive lava flows occur at the middle of the volcanic section in the area. Plagioclase of anorthite ($An_{95}$) to andesine ($An_{46}$) composition, pyroxene, amphibole and opaque minerals make up the primary minerals. Plagioclase generally shows fine to medium grained, anhedral to subhedral and irregularly aligned but occasionally show moderate alignment which probably may be linked to flow structure. Amphibole shows fine to medium grained textures, mostly twisted with the primary versions (amphibole 1) occurring in the matrix with primary plagioclase which is fine grained, and may as well be linked to flow structure. Later amphiboles are of two generations (amphibole 2 and 3). The former is medium grained (occasionally coarse grained) and occurs as an overprint on primary plagioclase and amphibole. The latter is medium grained, anhedral to sub-rounded and appears colloidal.

The major rocks are intruded by minor rocks of different thickness and textures which are medium to coarse grained, porphyritic with irregular alignment. A cross cutting structure observed in the field suggests a generational relationship between the intrusives. The cross cutting intrusives (G6 and G7) are classified as gabbroic diorite (first generation) and diorite (second generation) and the coarser grained (sheared) intrusive (G14) as granodiorite (Fig. 4.12a). The primary minerals of the intrusives comprise of plagioclase of labradorite to andesine composition ($An_{52}$ - $An_{48}$), amphibole and pyroxene with tourmaline, actinolite, apatite and garnet as accessory minerals. The gabbroic diorite is moderately foliated with primary fine grained plagioclase and amphiboles occupying the foliations. The diorite is porphyritic with medium grained plagioclase and medium to coarse grained amphiboles. The coarse grained granodiorite has aligned medium grained plagioclase and medium to coarse grained amphibole (Fig. 4.10a to c). Like the host rocks, the amphiboles in the intrusives are of different generations which were probably introduced at different stages of the rock formation. The primary amphiboles (amphibole 1) are fine to medium grained, occasionally twisted and occur in the matrix with primary plagioclase. Later amphiboles are of three types (amphiboles 2, 3 and 4). Amphibole 2 is coarse grained, granular, elongated

and overprints primary plagioclase and amphiboles (Fig. 4.7c). Amphibole 3 is coarse grained, sub-rounded, appears colloidal and may be metamorphic as it occurs close to a vein. Amphibole 4 is coarse grained, granular, elongated, fractured and might have come with a vein (Fig. 4.8a).

Generally, quartz, sericite and carbonate are alteration products of plagioclase. Amphibole is partially altered to chlorite and epidote. These minerals together with actinolite and garnet suggest greenschist facies of the Barovian series outlined by Miyashiro, (1973a). Therefore, the general metamorphism of the rocks is in the greenschist facies. John *et al.* (1999) are of the opinion that majority of the rocks within the south of the Ashanti belt have been subjected to greenschist facies metamorphism and are retrograde from amphibolite facies which occur near intrusives. The gabbroic diorite contains xenolith of amphibolite (Fig. 4.8e). This rock is near the contact with the belt granitoid which occurs towards the west at Dixcove area and may suggest metamorphism to amphibolite facies. Amphibole shows strong replacement by pyroxene and opaque minerals. This trend is common in the gabbroic diorite (Fig. 4.7c). Opaque minerals probably are alteration products of iron bearing silicates. In some cases, opaque minerals typically magnetite are generated from the conversion of amphibole to pyroxene which is effected by the decomposition of the hydroxyl group at elevated temperatures (Hatch *et al*., 1972). The resulting opaque minerals may be as a result of oxidation (and/or sulphidation) of iron components of the amphibole mineral.

The host rocks (basalt and andesite) in the study area are metamorphosed. The AFM diagram (Fig. 4.13a) puts the basalt, gabbroic diorite and granodiorite at the tholeiitic region and the diorite and andesite at the calc-alkaline region. Kleinschrot *et al*. (1994) are of the opinion that tholeiitic lavas gradually grade into calc-alkaline andesitic flows. A trend which was observed in this study (Figs 4.13 and 4.14). Whole rock geochemistry results are presented in Appendix 1. From the plot of $MgO/SiO_2$ wt.% (Fig. 4.13d), all rock types from this study area could be considered as low magnesian rocks although a sample of the basalt showed higher MgO enrichment. The trend of MgO variation with $SiO_2$ in this study is similar to that observed by Sylvester and Attoh, (1992) for the tholeiitic basalt from the Dixcove area but quite the opposite for the andesite. On the basis of $Na_2O$ and $K_2O$ variations with $SiO_2$ plots (Fig. 4.15a and b), within the basalt, there is a general depletion of $K_2O$ and $Na_2O$ contents relative to their content in the andesite. On comparison, the

andesite in this study showed significantly higher $K_2O$ content than that observed by Sylvester and Attoh, (1992) at the Dixcove area. The characteristic < 0.5 wt. % $K_2O$ content and the tholeiitic signature of the studied basalts may suggest petrogenic features rather than alteration. Among the intrusives, the diorite showed variable major oxide geochemistry. Whereas two samples of the diorite, gabbroic diorite and granodiorite showed reduced $K_2O$ and $Na_2O$ contents, two other diorite samples showed relatively enriched $K_2O$ and $Na_2O$. According to Dampare *et al*. (2005), some mafic intrusives are typically hybrid rocks which may have formed by the interaction between granitoid magma and the host mafic rocks. Loh and Hirdes, (1992) believes the mafic rocks from the Princes Town area may show variations in geochemistry relative to others formed through a normal differentiation activity from a magma. This may hold true for the diorite from the study area and may even be extended to other rock types. For example, the granodiorite in this study is tholeiitic compared to the calc-alkaline from Dampare *et al*. (2005). This may be explained as an assimilation of more mafic minerals by the granodiorite from the mafic basalt. The bivariant plots (Figs. 4.13, 3.14, 4.15, 4.16) suggest a fractionation trend from tholeiitic basalt through gabbroic diorite, granodiorite, andesite and diorite.

Since the Birimian rocks have been subjected to greenschist facies metamorphism, a possible exchange between major elements and metamorphic fluids may have taken place. It is therefore cautioned that major element chemical data be treated with care (Abouchami *et al*., 1990). On the other hand, trace elements typically rare earth elements (REE) are strongly resistant to metamorphism and hydrothermal activities, hence are recommended in assessing the various characteristics of rocks (Michard, 1989). All rock types from this study are LREE depleted (La/Sm chondrite normalised ratios of basalt = 0.8 to 2.5; andesite = 2.03; diorite = 1.95 to 3.1; gabbroic diorite = 0.9 to 2.05; granodiorite = 1.66) (Appendix B). The diorite, basalt and andesite are fairly enriched in HREE (La/Yb chondrite normalised ratios of diorite = 4.96 to 10.74; basalt = 1.8 to 8.7; andesite = 8.28). Gabbroic diorite and granodiorite are depleted in HREE (La/Yb chondrite normalised ratios of gabbroic diorite = 1.51 to 3.75; granodiorite = 4.10) (Fig. 4.19a). There is a general negative Eu anomaly with Eu/Eu* ratios of basalt = 0.93 to 1.15; andesite = 1.03; diorite = 0.95 to 1.06; gabbroic diorite = 0.75 to 1.06; granodiorite = 1.05. Negative Ce anomaly occurs in all rock types (Fig 4.19a.). Similar NMORB normalised REE patterns were observed by Sylvester and Attoh, (1992).

Perfit *et al*. (1980) are of the assertion that with high $Al_2O_3$ content and low Ti, REE and high field strength elements, most Birimian basalts plot as an intermediate between mid-oceanic ridge basalt (MORB) and island arc environments. This trend was observed in this study (Fig. 4.17a). High Ba and Sr contents with corresponding low to moderate $TiO_2$ content may also suggest arc magma affinities (Sylvester and Attoh, 1992). Negative Ce anomaly has been described by Hole *et al*., (1984) as due to a limited amount of subducted sediment in the source magma. Sylvester and Attoh, (1992) also believe negative Ce anomaly may represent fractionation from fluids arising from dehydrating subducted slab. Therefore, the host rocks originally formed relative to a subduction zone activity supporting previous studies by (Grenholm 2005; Beziat *et al.,* 1999; Sylvester and Attoh, 1992) but Abouchami *et al.* (1990) support plume volcanism. The intrusives plot in the volcanic arc + syncollision granite region (Fig. 4.18). However, the gabbroic diorite and the granodiorite may have been deposited as mantle fractionates as the diorite probably intruded prior to plate collision (Fig. 4.19b).

The relationship between $Na_2O$, $K_2O$ and the alteration index (AI) for rocks from Butre area is shown in Figs. 4.20a and b. The plot displays an increase-decrease pattern between AI, $K_2O$ and $Na_2O$. For $Na_2O$ against AI, an increase in AI leads to a decrease in $Na_2O$ and tends to favour sericite-chlorite formation. In this study, the rocks plot along the dolomite-ankerite region but also show epidote-calcite and to some extent chlorite-sericite alteration. Higher AI values may either be associated with increased $K_2O$ in which case sericite alteration is favoured or may be accompanied by a decrease in $K_2O$ in which case chlorite alteration is favourable. In this study, the rocks plot along the dolomite-ankerite-calcite-epidote join and the dolomite-ankerite-chlorite join with or without sericite. On the basis of low $K_2O$ content recorded for the rocks in this study, chlorite alteration may be higher than sericite alteration. The chlorite-carbonate-pyrite index (CCPI) plotted against the AI is useful to outline hydrothermal alteration from diagenetic/metamorphic alteration which are distinguished with a line joining the epidote and k-feldspar of the box plot. The least altered rocks are bound by AI values of 20 to 65 and CCPI values of 15 to 45, which may vary for each volcanic rock on the basis of their composition (Large *et al*., 2001).

For this study, most of the rocks (basalt, gabbroic diorite and granodiorite) plotted above the least altered box with the diorite, andesite (and a sample of the gabbroic diorite) plotting in the least altered box. It was pointed out by Large *et al*. (2001) that, if the intensity of

sericite and chlorite is low, they may be inferred from greenschist metamorphic minerals rather than hydrothermally related. In this study, the rocks plotted in the hydrothermal region of the box plot although the sericite and chlorite alteration may not be intense but significant. Diagenetic alteration of marine volcanic rocks may lead to clays, zeolites, and feldspars formation but for greenschist metamorphosed terrains, it is evident by albite, K feldspar, calcite, and epidote alterations (Gifkins and Allen, 2001). Hence, albite, Kfeldspar, calcite, and epidote are common diagenetic minerals and plot in the diagenetic region whiles the hydrothermal region is bound by minerals such as sericite, chlorite, pyrite, dolomite, and ankerite. Majority of the rocks in the study area (e.g. basalt, gabbroic diorite and granodiorite) plotted along the dolomite-ankerite join towards the chlorite-pyrite region. Hence, these rocks have been affected to some extent, by hydrothermal activities. The granodiorite also shows epidote-calcite alteration which could be metamorphic rather than diagenetic since the epidote and the carbonate encountered in the petrographical studies were all alteration minerals. The diorite in addition, show sericite-carbonate alteration. In summary, the box plot suggests a general dolomite-ankerite-chlorite±pyrite for the basalt and gabbroic diorite, epidote-calcite-dolomite-ankerite for the granodiorite and dolomite-ankerite-sericite±epidote±calcite for the diorite. The chlorite observed in petrographical studies were fine grained alteration mineral of amphibole and hence not intense just as the sericite. These minerals are therefore metamorphic and related to greenschist facies metamorphism.

The successive emplacement of later intrusives might have introduced some gangue minerals and opaque minerals in the earlier emplacements. The emplacement of gabbroic diorite might have been accompanied by arsenopyrite as this rock type contains arsenopyrite as the most occurring opaque mineral which is also common in the basalt (Fig 4.9a). Granodiorite might have played a role in the introduction of carbonate, pyrite and quartz (Fig 4.13a, and 4.12a). The diorite probably might have introduced quartz and pyrite as it contains pyrite as the most occurring opaque mineral (4.9f). Hydrothermal fluids which might be related to the emplacement of the major belt granitoids further west of the study area may be responsible for the temperature needed for the conversion of amphibole to pyroxene which was accompanied by some opaque minerals. Pyrite and magnetite are probable minerals from this activity associated with quartz veins overprinted by opaque minerals (Fig. 4.4a and b; 4.7 c and e).

There are two stages of metamorphism - amphibolite facies and greenschist facies. Amphibolite facies stage introduced amphibole + plagioclase + garnet + epidote + quartz + magnetite (Fig 4.11c). The greenschist facies stage introduced minerals such as amphibole + epidote + chlorite + sericite + carbonate + haematite + pyrrhotite (Fig 4.2a, 4.8a and 4.13b). Hydrothermal activity introduced carbonate + quartz + magnetite + pyrite (Fig. 4.7e).

Gold in this study is trace. However, it has been reported by various authors example (Griffis *et al*., 2008 and Osae *et al*., 1999) that gold is usually associated with arsenopyrite, pyrite and to some extent pyrrhotite in metasedimentary and metavolcanic rocks of the Birimian. This arsenopyrite-pyrite-pyrrhotite association is mostly intricate in nature with gold occurring in fractures and surfaces of these minerals. This was also reported by Osae *et al*. (1999) that in some instances, visibility of gold in arsenopyrite is only brought to light under higher magnification under the microscope or as in the case of Oberthür *et al*. (1997), secondary ion mass spectroscopy. With arsenopyrite and pyrite as the major opaque minerals, the study area may be gold mineralised but a higher magnifying microscope is needed for their detection.

# CHAPTER 6

## CONCLUSIONS AND RECOMMENDATIONS

### 6.1 Conclusions

The major rocks in the study area are basalt and andesite which show pillow structures, fractured and massive flows. The major rocks are intruded by gabbroic diorite, diorite and granodiorite. These are metamorphosed volcanic rocks which show tholeiitic and calc-alkaline trends. The differentiation trend of the rocks is from tholeiitic basalt through gabbro-diorite, granodiorite, andesite and diorite. These rocks are comagmatic and were emplaced relative to a subduction zone.

Generally, the rocks have been altered with quartz, sericite and carbonates being alteration products of plagioclase whereas chlorite and epidote were derived from partially altered amphibole. Alteration of plagioclase to sericite, quartz and carbonate followed granodiorite emplacement. The mineralogical change from amphibole to pyroxene probably also followed granodiorite emplacement.

Amphibolite facies metamorphism preceded greenschist facies metamorphism as xenoliths in gabbro-diorite contain amphibole + plagioclase + garnet + epidote. The greenschist facies metamorphic mineral package is generally epidote + chlorite + sericite + carbonate.

Arsenopyrite accompanied emplacement of gabbroic diorite whereas pyrite accompanied emplacement of diorite and granodiorite. The amphibolite facies metamorphism introduced magnetite whilst haematite and pyrrhotite accompanied the greenschist facies metamorphism. Earlier ore minerals could have been consumed to form later minerals.

All rock types are LREE depleted (La/Sm chondrite normalised ratios of basalt = 0.8 to 2.5; andesite = 2.03; diorite = 1.95 to 3.1; gabbroic diorite = 0.9 to 2.05; granodiorite = 1.66). The diorite, basalt and andesite are fairly enriched in HREE but gabbroic diorite and granodiorite are depleted in HREE. There is also a general negative Eu and Ce anomaly in all rock types.

Enriched total FeO wt. %, MgO wt. % and CaO wt. % in the basalt, granodiorite and gabbroic diorite may be the effect of chloritisation and carbonitisation. $SiO_2$ enrichment in diorite and granodiorite may be due to silicification, $K_2O$ and $Al_2O_3$ enrichment in diorite and andesite may be the result of sericitisation.

## 6.2 Recommendations

Since the rocks are highly altered, it was difficult to identify the primary minerals. It is therefore recommended that,

- Further work should employ the use of electron microscope for mineral identification.
- The use of mineral chemistry would be useful to identify types of minerals and their relationship.
- Ore mineralogical studies using microprobe could show the distinction between the various ore minerals and how they relate to the modification of the rocks during the volcanism, intrusions and metamorphisms.
- Geochemical work should target how the various stages of intrusions and metamorphism changed the composition of major and trace elements in the rocks.

# REFERENCES


Abouchami, W., Boher, M., Michard, A. and Albarede, F. (1990), "A major 2.1 Ga Event of Mantle Magmatism in West Africa, an Early Stage Crustal Accretion", *Geophysical Research Bulletin*, Vol. 95, pp. 17605-17629.

Adadey, K., Clarke, B., Théveniaut, H., Urien, P., Delor, C., Roig, J.Y. and Feybesse, J.L. (2009), "Geological map explanation-Map, sheet 0503 B (1:1 000 000), CGS/BRGM/Geoman", *Geological Survey Department of Ghana (GSD), No MSSP/2005/GSD/5a.*

Allibone, A., Hayden, P., Cameron, G. and Duku, F. (2004), "Paleoproterozoic Gold Deposits Hosted by Albite- and Carbonate-Altered Tonalite in the Chirano District, Ghana, West Africa", *Economic Geology Vol. 99, pp. 479–497.*

Allibone, A., McCuaig T. C., Harris D., Etheridge, M., Munroe, S. and Byrne, D. (2002a), "Structural Controls on Gold Mineralisation at the Ashanti Gold Deposit Obuasi, Ghana", *Economic Geology, Special Publication, Vol. 9, pp. 60 – 94*.

Asihene, K. A. B. and Barning, K. (1975), "A Contribution to the Stratigraphy of the Birimian System of Ghana, West Africa", *Ghana Geological Survey Report 75/5, Accra, 30 pp.*

Attoh, K. (1980). "Structure, Stratigraphy, and some Chemical characteristics of an Early Proterozoic (Birimian) Volcanic belt, northeastern Ghana", *Current Research, Part C, Geological Survey Canada Paper 80-1C, pp. 69 - 80.*

Attoh, K., Evans, M. J. and Bickford, M. E. (2006), "Geochemistry of an Ultramafic-Rodingite Rock Association in the Palaeoproterozoic Dixcove Greenstone Belt Southwestern Ghana", *Journal of African Earth Sciences, pp. 333 - 346.*

Berge, J. (2011), "Paleoproterozoic, turbidite-hosted, gold deposits of the Ashanti gold belt (Ghana, West Africa): Comparitive analysis of turbidite-hosted gold deposits and an updated genetic model", *Ore Geology Reviews, 39, 91-100.*

Bessoles, B. (1977), "Le Craton Ouest Africain Mémoire. Bureau Recherque Géologique Minière, Orléans", *Géologie de l'Afrique, Vol. 1, 88, 402 pp.*

Beziat D., Bourges F., Debat P., Lompo M., Martin F. and Tollon F. (1999), "Laboratoire de Mine´ralogie et Cristallographie", *UMR* 5563, *Uni6ersite´ Paul Sabatier*, 39 *Alle´es Jules Guesde*, 31000 *Toulouse Cedex, France.*

Craw, D. and Findlay, R. H. (1984), "Hydrothermal alteration of Lower Ordovician granitoids and Devonian Beacon Sandstone at Taylor Glacier, McMurdo Sound, Antarctica, New Zealand", *Journal of Geology and Geophysics, 27:4, 465-475, DOI: 10.1080/00288306.1984.10422266.*

Dampare S. B., Shibata T., Asiedu D. K., Osae S. and Banoeng-Yakubo B. (2005), "Geochemistry of Paleoproterozoic metavolcanic rocks from the southern Ashanti volcanic belt, Ghana: Petrogenetic and tectonic setting implications", *Precambrian Research 162 (2008) 403-423.*

Davis, D.W., Hirdes, W., Schaltegger, E. and Nunoo, E.A., (1994), "U/Pb age constraints on deposition and provenance of Birimian and gold-bearing Tarkwaian sediments in Ghana, West Africa", *Precambr. Res.*, **67**, 89-107.

Deer, W. A., Howie, R. A. and Zussman, J. (1966), "An Introduction to the Rock Forming Minerals, Third ELBS Impression 198", *Longman Group Limited, ISBN: 0 582 40716.8*

Derakhshani, R and Abdolzadeh, M. (2009)., "Geochemistry, Mineralisation and Alteration Zones of Darrehzar Porphery Copper Deposit, Kerman, Iran", *Journal of Applied Science 9 (9): 1628-1646.*

Eastoe, C.J., Solomon, M., and Walshe, J.L. (1987), "District-scale alteration associated with massive sulfide deposits in the Mount Read Volcanics, western Tasmania", *Economic Geology, v. 82, p. 1239–1258.*

Eisenlohr, B.N. and Hirdes, W. (1992), "The structural development of the early Proterozoic Birimian and Tarkwaian rocks of southwest Ghana, West Africa", *J. Afr. Earth Sci. 14, 313–325.*

Feybesse, J.-L., Billa, M., Guerrot, C., Duguey, E., Lescuyer, J.-L., Milesi, J.-P. and Bouchot, V. (2006), "The Paleoproterozoic Ghanaian province: Geodynamic model and ore controls, including regional stress modelling". *Precambrian Research, 149, 149-196.*

Gifkins, C.C., and Allen, R.L. (2001), "Textural and chemical characteristics of diagenetic and hydrothermal alteration in glassy volcanic rocks: Examples from the Mount Read Volcanics, Tasmania", *ECONOMIC GEOLOGY*, Vol. 96, p. 973–1002.

Griffis, R. J., Barning, K., Agezo, F. L. and Akosah, F. K. (2002), "Gold deposits of Ghana", *Minerals Commission, Accra, 432pp.*

Hatch, F. K., Wells, A. K. and Wells, M. K., (1972), "Petrology of the igneous rock", *thirteenth ed., George Allen &Unwin Ltd. Pp 98, 99.*

Hirdes, W., Davis, D. W. and Eisenlohr, B. N. (1992), "Reassessment of Proterozoic granitoid ages in Ghana on the basis of U/Pb zircon and monazite dating", *Precambrian Res. 56, 89–96.*

Hirdes, W., Senger, R., Adjei, J., Efa, E., Loh, G. and Tettey, A. (1993), "Explanatory notes for the geological map of southwest Ghana – 1:100,000 (Wiawso, Asafo, Kukuom, Sunyani and Berekum sheets)", *Geologische Jahrbuch, Reihe B, 83, 139pp*.

Hole, M. J., Saunders, A. D., Marriner, G. F. and Tarney, J. (1984), "Subduction of pelagic sediments: implications for the origin of Ce-anomalous basalts from the Mariana Islands", *Jour. Geol. Soc. London, v. 141, p. 453-472.*

Hutchison, C. S. (1974), "Laboratory Handbook of Petrographic Techniques", John *Wiley and Sons Press, 527 pp.*

Irvine, T. N. and Baragar, W. R. A. (1971), "A guide to the chemical classification of the common volcanic rocks", *Canadian Journal of Earth Sciences* **8,** 523–548.

Ishikawa, Y., Sawaguchi, T., Iwaya, S. and Horiuchi, M. (1976), "Delineation of prospecting targets for Kuroko deposits based on modes of volcanism of underlying dacite and alteration halos", *Mining Geology, v. 26, p. 105–117* (in Japanese with English abs.).

John, T., Kleimd, R., Hirdes, W. and Loh, G. (1999), "The Metamorphic Evolution of the Palaeoproterozoic (Birimian) Volcanic Ashanti belt (Ghana, West Africa)", *Precambrian Research, Vol. 98, pp. 11 – 30.*

Kaur, P., Chaudril, N., Hoffman A. W., Raczek I., Okrusch M., Skora S. and Baumgartner, P. (2012), "Two-Stage, Extreme Albitisation of A-type Granite from Rajasthan, NW India", *Journal of Petrology*, Vol 53, Number 5, 919-948.

Kesse, G., (1985), "The Mineral and Rocks Resources of Ghana. A.A. Balkema, Rotterdam Boston", p. 609.

Kumral, M., Abdelnasser, A. and Budakoglu M. (2016), "Geochemistry of Hydrothermal Alteration Associated with Cenozoic Intrusion-Hosted Cu-Pb-Zn Mineralization at Tav¸sanlı Area, Kütahya, NW Turkey, *Minerals 2016, 6, 13*.

Large R., Gemmell J. B., Paulick, H., and Huston D. L. (2001), "The Alteration Box Plot: A Simple Approach to Understanding the Relationship between Alteration Mineralogy and Lithogeochemistry Associated with Volcanic-Hosted Massive Sulfide Deposits", *Economic Geology Vol. 96, 2001, pp. 957–971*

Loh, G., Hirdes,W. (1999), "Explanatory notes for the geological map of southwest Ghana", 1:100,000: sheets Sekondi (0402A) and Axim (0403B): *Ghana. Geol. Surv. Bull. 49, 149.*

Michard, A. (1989), "Rare-earth element systematics in hydrothermal fluids", Geochim. Cosmochim. Acta, 53, 745-750.

Middlemost, E. A. K. (1985), "Naming materials in the magma/igneous rock system", *Earth-Sciences Reviews* **37,** 215–224.

Oberthür T., Hirdes W., Höhndorf A., Mumm A. S., Vetter U., Weise r T., Davis D. W., Blenkinsop T.G., Amanor J.A., and Loh G. (1995), "A Review of Gold Mineralisation in the Ashanti Belt of Ghana and its Relation to the Crustal Evolution of the Terrane", *Communs geol. Surv. Namibia, **10** (1995), 121-127*

Oberthür, T, Vetter, U., Davis, D.W. and Amanor, J.A. (1998), "Age constraints on gold mineralization and Paleoproterozoic crustal evolution in the Ashanti belt of southern Ghana", *Precambrian Research, 89, 129-143*.

Oberthür, T., Weiser, T., Amanor, J. A. and Chryssoulis, S. L. (1997), "Mineralogical siting and distribution of gold in quartz veins and sulphide ores of the Ashanti mine and other deposits in the Ashanti belt of Ghana: genetic implications", Mineral. Deposita, 32, 2–15.

Amponsah O. P., Salvi S., Beziat D., Siebenaller L., Baratoux L., and Jessell M. W. (2015), "Geology and geochemistry of the shear-hosted Julie deposit", NW Ghana. *Journal of African Earth Sciences 112 (2015) 505-523.*

Osae S., Kase K., and Yamamoto M. (1999), "Ore Mineralogy and Mineral Chemistry of the Ashanti Gold Deposit at Obuasi, Ghana", *Resource geology, vol. 49, no. 1, 1–11*

Pearce, J. A. (1996), "A user's guide to basalt discrimination diagrams. In: Wyman, D. A. (ed.) Trace Element Geochemistry of Volcanic Rocks: Applications for Massive Sulphide Exploration", Geological Association of Canada, *Short Course Notes 12, 79–113.*

Perrouty S., Aillères L., Jessell M. W., Baratoux L., Bourassa Y. and Crawford B. (2012). Revised Eburnean geodynamic evolution of the gold-rich southern Ashanti Belt, Ghana, with new field and geophysical evidence of pre-Tarkwaian deformations,

Perrouty, S., Jessell, M.W., Bourassa, Y., Miller, J., Apau, D., Siebenaller, L., Velásquez, G., Baratoux, L., Aillères, L., Béziat, D. and Salvi, S. (2015), "The Wassa deposit: A poly-deformed orogenic gold system in southwest Ghana – Implications for regional exploration", *Journal of African Earth Sciences, http:// dx.doi.org/10.1016/j.jafrearsci.2015.03.003.*

Perfit, M. R., Gust, D.A., Bence, A .E., Arculus, R .J. and Taylor, S .R. (1980), "Chemical characteristics of island-arc basalts:- implications of mantles sources Chem", Geol., 30, 227-256.

Rajah, S. S., Fateh, C. and Singh S. D. (1977)", The granitoids and mineralisation of the Eastern Belt of Penisula Malaysia, *Geological Society of Malaysia Bulletin 9, pp. 209-232.*

Schardt, C., Cooke, D.R., Gemmell, J.B., and Large, R.R. (2001), "Geochemical modeling of the zoned footwall alteration pipe, Hellyer volcanic-hosted massive sulfide deposit, western Tasmania, Australia", *Economic geology, v. 96, p. 1037–1054.*

Schmid R., Fettes D., Harte B., Davis E., and Desmond J. (2007), "A systematic nomenclature for metamorphic rocks. How to name metamorphic rock". Recommendations by the IUGS Subcommission on the systematics of metamorphic rocks. SCMR website (www.bgs.ac.uk/SCMR)

Smith A. J. B., Henry G., and Frost-Killian S. (2016), "A review of the Birimian Supergroup- and Tarkwaian Group-hosted gold deposits of Ghana", , *IUGS, Vol. 39, No. 2.*

Leube, A., Hirdes, W., Mauer, R., and Kesse, G. (1990), "The early proterozoic birimian supergroup of ghana and some aspects of its associated gold mineralization", *Precambrian Research, 46:139–165.*

Sylvester P. J. and Attoh K. (1992), "Lithostratigraphy and Composition of 2.1 Ga Greenstone Belts of the West African Craton and Their Bearing on Crustal Evolution and the Archean-Proterozoic Boundary", *Journal of Geology, volume 100, p. 377-393*

Tetteh, G. M. and Effisah-Otoo, E. (2017), "Petrography and Geochemistry of some Granitoids associated with Gold Mineralisation at Mpohor area in southeastern Ashanti Belt of the Birimian, Ghana", *Ghana Mining Journal, Vol. 17, No. 1, pp. 31 - 42.*

Verma, P. K., (2010), "Optical Mineralogy", *Ane Books Pvt Ltd, ISBN: 978-93-8015-608-8.*

Winchester, J. A., Floyd, P. A. (1977**), "**Geochemical discrimination of different magma series and their differentiation products using immobile elements", *Chemical Geology DOI: 10.1016/0009-2541(77)90057-2 CITATIONS 3,419*

Yao, Y. and Robb, L.J. (2000), "Gold mineralization in Palaeoproterozoic Granitoids at Obuasi, Ashanti region, Ghana: ore geology, geochemistry and fluid characteristics. *South African Journal of Geology 103, 255–278*

Kleinschrot, D., Bröcker, M., Okrusch, M. and Franz, L. (1994), "Protores and country rocks of the Nsuta manganese deposit (Ghana)", *N. Jb.Miner. Abh. 168: 67-108; Stuttgart 1994.*

Micko, J., Tosdal, R. M., Bissig, T., Chamberlain, C. M. and Simpson K. A. (2014), "Hydrothermal Alteration and Mineralization of the Galore Creek Alkalic Cu-Au Porphyry Deposit, Northwestern British Columbia, Canada", *Society of Economic Geologists, Inc. Economic Geology, v. 109, pp. 891–914.*

Wright, J.B., Hastings, D.A., Jones, W.B. and Williams, H.R. (1985), "Geology Mineral Resources of West Africa", *Allen and Unwin, London, 187pp.*

Large, R.R., Gemmell, J.B., Paulick, H. and Huston, D.L. (2001), "The alteration box plot: A simple approach to understanding the relationship between alteration mineralogy and lithogeochemistry associated with VHMS deposits", *Econ. Geol. 2001, 96, 957–972.*

Miyashiro, A. (1973), "Metamorphism and Metamorphic belts", *Allen and Unwin, London,492pp.*

Petersson, A., Scherstén, A. and Gerdes A. (2018), "Extensive reworking of Archaean crust within the Birimian terrane in Ghana as revealed by combined zircon U-Pb and Lu-Hf isotopes", *Geoscience Frontiers 9 (2018) 173-189.*

Amponsah, P.O., Salvi, S., Béziat, D., Baratoux, L., Siebenaller, L., Nude, P.O., Nyarko, R.S. and Jessell, M.W. (2016), "The Bepkong gold deposit, northwestern Ghana", *Ore Geol. Rev. 78, 718–723.*

Yoa, Y., Murphy, P.J. and Robb, L.J. (2001), "Fluid Chaarqcteristics of granitoid-hosted Gold deposit in the Birimian terrane of Ghana: A fluid Inclusion Microthermometric and Raman spectroscopic study", *Economic Geology, 96, 1611-1643.*

Sun S.S. and McDonough W.F. (1989), "Chemical and isotopic systematics of oceanic basalts: implications for mantle composition and processes". *Geological Society of London special publication; v. 42; p. 313-345.*

Pearce, J.A. (2008), "Geochemical Fingerprinting of Oceanic basalts with applications to ophiolite classification and the search for Archean Oceanic crust". *Lithos 100 (1-4), 14-48.*

Pearce, J.A. and Norry, M.J. (1979), "Petrogenetic Implications of Ti, Zr, Y and Nb variations in volcanic rock", *Contributions to mineralogy and petrology 69 (1), 33-47.*

Hollocher, K., Robinson, P., walsh, E. and Roberts, D. (2012), "Geochemistry of Amphibolite-facies volcanics and gabbros of the Storen Nappe in extensions west and southwest of Trondheim", Western Gneiss Region, Norway: A Key to correlations. *American Journal of science 312 (4) 357-416.*

Batchelor, R.A. and Bowden, P. (1985), "Petrogenetic interpretation of granitoid rock series using multicationic parameters*", Chemical Geology, Vol. 48, issues 1-4*.

Pearce, J.A. and Harris, N. (1984), "Trace Element Discrimination Diagrams for the Tectonic interpretation of Granitic rocks", *Journal of Petrology, 25:956-983.*

# APPENDICES

## APPENDIX A

### Table A.1 Whole rock XRF composition of representative samples from Butre area

| Sample ID | G1 | G3 | G4 | G5 | G6 | G7 | G8 | G9 | G10 | G11 | G12 | G13 | G14 |
|---|---|---|---|---|---|---|---|---|---|---|---|---|---|
| Oxide wt.% | | | | | | | | | | | | | |
| $SiO_2$ | 48.6 | 62.7 | 62.6 | 49.6 | 56.2 | 58.6 | 56.6 | 47.7 | 58.3 | 52.6 | 61.9 | 52.6 | 65 |
| $Al_2O_3$ | 14.8 | 15.45 | 14.9 | 14.1 | 13.4 | 14.5 | 12.25 | 15.25 | 13.25 | 14.45 | 11.1 | 12.6 | 12.9 |
| $Fe_2O_3$ | 10.65 | 5.56 | 5.84 | 13.35 | 10.4 | 8.09 | 9.49 | 10.95 | 9.28 | 11.6 | 5.56 | 11.25 | 7.15 |
| CaO | 13.65 | 3.03 | 4.69 | 11.05 | 15.35 | 6.95 | 8.29 | 8.86 | 5.76 | 10.15 | 4.96 | 13.35 | 12.65 |
| MgO | 6.7 | 2.87 | 3.57 | 5.46 | 2.21 | 4.16 | 7.5 | 10.15 | 7.38 | 5.47 | 2.68 | 5.19 | 0.89 |
| $Na_2O$ | 2.1 | 3.95 | 4.11 | 1.35 | 0.13 | 3.79 | 1.94 | 2.6 | 2.78 | 2.11 | 3.46 | 0.23 | 0.39 |
| $K_2O$ | 0.28 | 2.26 | 2.02 | 0.22 | 0.04 | 0.49 | 0.11 | 0.37 | 0.04 | 0.13 | 1.12 | 0.05 | 0.21 |
| $Cr_2O_3$ | 0.066 | 0.033 | 0.032 | 0.052 | 0.064 | 0.022 | 0.062 | 0.095 | 0.044 | 0.08 | 0.037 | 0.085 | 0.058 |
| $TiO_2$ | 0.64 | 0.46 | 0.46 | 1.19 | 0.82 | 0.67 | 0.5 | 0.69 | 0.52 | 0.92 | 0.43 | 0.86 | 0.42 |
| MnO | 0.16 | 0.08 | 0.09 | 0.15 | 0.11 | 0.1 | 0.14 | 0.16 | 0.12 | 0.13 | 0.15 | 0.13 | 0.06 |
| $P_2O_5$ | 0.16 | 0.2 | 0.19 | 0.07 | 0.07 | 0.28 | 0.12 | 0.09 | 0.11 | 0.11 | 0.47 | 0.06 | 0.04 |
| SrO | 0.03 | 0.05 | 0.06 | 0.02 | 0.04 | 0.04 | 0.04 | 0.02 | 0.02 | 0.03 | 0.07 | 0.04 | 0.05 |
| BaO | 0.02 | 0.1 | 0.08 | 0.01 | <0.01 | 0.02 | 0.01 | 0.01 | <0.01 | 0.01 | 0.03 | <0.01 | 0.01 |
| LOI | 2.08 | 3.32 | 1.74 | 2.47 | 1.48 | 1.98 | 2.65 | 3.32 | 3.49 | 2.63 | 7.37 | 2.49 | 1.38 |
| **Total** | **99.94** | **100.06** | **100.38** | **99.09** | **100.31** | **99.69** | **99.7** | **100.27** | **101.09** | **100.42** | **99.34** | **98.94** | **101.21** |
| Trace Element (ppm) | | | | | | | | | | | | | |
| Ba | 140.5 | 915 | 746 | 58.8 | 18.8 | 191 | 62.3 | 135.5 | 17.2 | 56.3 | 256 | 21.9 | 80.7 |
| Ce | 30 | 30.5 | 30.2 | 6.3 | 6.2 | 43.4 | 15.5 | 12.4 | 14.5 | 13.4 | 26.4 | 7.3 | 5.7 |
| Cr | 470 | 260 | 260 | 380 | 470 | 160 | 470 | 690 | 280 | 560 | 270 | 590 | 390 |
| Cs | 0.11 | 1.03 | 1.08 | 0.12 | 0.06 | 0.12 | 0.09 | 0.22 | 0.05 | 0.07 | 2.7 | 0.04 | 0.07 |
| Dy | 2.36 | 2.13 | 1.81 | 3.38 | 2.39 | 2.96 | 2.27 | 2.21 | 1.94 | 2.17 | 2.68 | 1.99 | 0.99 |
| Er | 1.38 | 1.13 | 1.02 | 1.8 | 1.62 | 1.41 | 1.2 | 1.51 | 1.19 | 1.53 | 1.3 | 1.19 | 0.61 |
| Eu | 1.18 | 0.96 | 0.87 | 0.76 | 0.46 | 1.32 | 0.73 | 0.79 | 0.62 | 0.77 | 1.2 | 0.73 | 0.36 |
| Ga | 14.3 | 20.3 | 19 | 16 | 16.1 | 17.3 | 14.7 | 14 | 10.5 | 12 | 14.8 | 12 | 14.8 |
| Gd | 2.95 | 2.58 | 2.52 | 2.69 | 1.97 | 3.61 | 2.08 | 2.15 | 1.85 | 2.73 | 3.52 | 2.12 | 1.01 |
| Hf | 1.2 | 3 | 2.8 | 1.3 | 0.8 | 3 | 1.8 | 1.4 | 1.5 | 1.3 | 2.2 | 1 | 0.7 |
| Ho | 0.41 | 0.39 | 0.37 | 0.59 | 0.47 | 0.57 | 0.44 | 0.46 | 0.45 | 0.47 | 0.49 | 0.46 | 0.28 |
| La | 14.1 | 14.9 | 14.5 | 2.9 | 3.3 | 20.4 | 6.9 | 5.5 | 6.5 | 5.3 | 11.7 | 2.9 | 2.9 |
| Lu | 0.2 | 0.15 | 0.15 | 0.25 | 0.27 | 0.25 | 0.19 | 0.22 | 0.19 | 0.21 | 0.14 | 0.18 | 0.09 |
| Nb | 3 | 3.3 | 3.2 | 1.5 | 1.6 | 3.3 | 2.2 | 3.2 | 2.2 | 5.9 | 5.3 | 2.6 | 1.5 |
| Nd | 17.3 | 14.7 | 14.2 | 6 | 5.6 | 24 | 8.4 | 7.7 | 8 | 8.2 | 14.2 | 5.9 | 3.8 |
| Pr | 4.04 | 3.82 | 3.89 | 1.11 | 1.02 | 5.86 | 2.08 | 1.67 | 1.85 | 1.79 | 3.38 | 1.03 | 0.76 |
| Rb | 5.3 | 59.3 | 55 | 4.2 | 0.6 | 8.4 | 1.8 | 8.8 | 0.4 | 2.7 | 50.3 | 0.7 | 3.9 |
| Sm | 3.59 | 2.98 | 3.07 | 2.26 | 1.79 | 4.61 | 2.1 | 2.05 | 2.08 | 2.14 | 3.6 | 2.02 | 1.09 |
| Sn | <1 | 1 | 1 | 1 | 1 | 1 | <1 | 1 | 1 | 1 | 4 | 1 | 1 |
| Sr | 292 | 436 | 486 | 215 | 379 | 365 | 328 | 237 | 150.5 | 278 | 593 | 356 | 417 |
| Ta | 0.2 | 0.3 | 0.4 | 0.2 | 0.2 | 0.4 | 0.3 | 0.3 | 0.2 | 0.3 | 0.3 | 0.3 | 0.2 |
| Tb | 0.33 | 0.36 | 0.3 | 0.5 | 0.38 | 0.54 | 0.35 | 0.36 | 0.32 | 0.28 | 0.59 | 0.34 | 0.16 |
| Th | 1.02 | 2.45 | 2.18 | 0.2 | 0.17 | 4.16 | 0.65 | 0.54 | 0.67 | 0.58 | 1.9 | 0.22 | 0.37 |
| Tm | 0.19 | 0.19 | 0.19 | 0.3 | 0.21 | 0.19 | 0.17 | 0.22 | 0.18 | 0.22 | 0.21 | 0.19 | 0.1 |
| U | 0.46 | 0.95 | 0.87 | 0.11 | 0.19 | 1.37 | 0.28 | 0.3 | 0.28 | 0.15 | 0.77 | 0.39 | 0.29 |
| V | 210 | 122 | 138 | 277 | 230 | 211 | 202 | 217 | 174 | 251 | 70 | 248 | 170 |
| W | 1 | 2 | 1 | 1 | 1 | 3 | 1 | <1 | <1 | 1 | 4 | <1 | 1 |
| Y | 11.7 | 11.3 | 9.9 | 16.7 | 13.6 | 14.9 | 11.2 | 12.8 | 9.8 | 11.2 | 12.3 | 11.4 | 5.8 |
| Yb | 1.1 | 1.05 | 1.21 | 1.83 | 1.48 | 1.29 | 1.25 | 1.24 | 0.89 | 1.18 | 0.96 | 1.27 | 0.48 |
| Zr | 48 | 109 | 108 | 42 | 35 | 105 | 67 | 54 | 60 | 43 | 81 | 39 | 27 |

## APPENDIX B

## SYMBOLOGY

**Table B.1 List of Symbols (after Schmid *et al.* 2007)**

| SYMBOL | NAME |
|---|---|
| Amp | Amphibole |
| Apy | Arsenopyrite |
| AI | Alteration index |
| Chl | Chlorite |
| CCPI | Chlorite-Carbonate-Pyrite index |
| Ep | Epidote |
| Hem | Haematite |
| Mag | Magnetite |
| Pl | Plagioclase |
| Po | Pyrrhotite |
| Px | Pyroxene |
| Py | Pyrite |
| Qtz | Quartz |
| Ser | Sericite |

## APPENDIX C

**Table C.1 GPS Locations and Numbers of samples collected at Butre area**

| GPS Coordinates | | Sample ID | | | |
|---|---|---|---|---|---|
| X | Y | Number of Samples Collected | | | |
| 620253 | 533281 | G1 | | | |
| 620418 | 532795 | G3 | G4 | G5 | |
| 620371 | 532727 | G6 | G7 | | |
| 626322 | 532691 | G8 | G9 | | |
| 626312 | 532681 | G10 | | | |
| 620215 | 532328 | G11 | G12 | G13 | G14 |

## APPENDIX D

**Table C.2 Chondrite Normalised REE values of Rocks from Butre area**

| | | | | Chondrite Normalised REE Values | | | | | | | | |
|---|---|---|---|---|---|---|---|---|---|---|---|---|
| | G1 | G5 | G9 | G11 | G12 | G3 | G4 | G7 | G10 | G6 | G8 | G13 | G14 |
| La | 59.4937 | 12.2363 | 23.2068 | 22.3629 | 49.3671 | 62.8692 | 61.1814 | 86.0759 | 27.4262 | 13.9241 | 29.1139 | 12.2363 | 12.2363 |
| Ce | 48.9396 | 10.2773 | 20.2284 | 21.8597 | 43.0669 | 49.7553 | 49.2659 | 70.7993 | 23.6542 | 10.1142 | 25.2855 | 11.9086 | 9.29853 |
| Pr | 43.5345 | 11.9612 | 17.9957 | 19.2888 | 36.4224 | 41.1638 | 41.9181 | 63.1466 | 19.9353 | 10.9914 | 22.4138 | 11.0991 | 8.18966 |
| Nd | 37.8556 | 13.1291 | 16.849 | 17.9431 | 31.0722 | 32.1663 | 31.0722 | 52.5164 | 17.5055 | 12.2538 | 18.3807 | 12.9103 | 8.3151 |
| Sm | 24.2568 | 15.2703 | 13.8514 | 14.4595 | 24.3243 | 20.1351 | 20.7432 | 31.1486 | 14.0541 | 12.0946 | 14.1892 | 13.6486 | 7.36486 |
| Eu | 20.9591 | 13.4991 | 14.032 | 13.6767 | 21.3144 | 17.0515 | 15.4529 | 23.4458 | 11.0124 | 8.17052 | 12.9663 | 12.9663 | 6.39432 |
| Gd | 14.8241 | 13.5176 | 10.804 | 13.7186 | 17.6884 | 12.9648 | 12.6633 | 18.1407 | 9.29648 | 9.8995 | 10.4523 | 10.6533 | 5.07538 |
| Dy | 9.5935 | 13.7398 | 8.98374 | 8.82114 | 10.8943 | 8.65854 | 7.35772 | 12.0325 | 7.88618 | 9.71545 | 9.22764 | 8.08943 | 4.02439 |
| Er | 8.625 | 11.25 | 9.4375 | 9.5625 | 8.125 | 7.0625 | 6.375 | 8.8125 | 7.4375 | 10.125 | 7.5 | 7.4375 | 3.8125 |
| Yb | 6.8323 | 11.3665 | 7.70186 | 7.32919 | 5.96273 | 6.52174 | 7.51553 | 8.01242 | 5.52795 | 9.19255 | 7.76398 | 7.8882 | 2.98137 |
| (Ce/Yb)n | 7.16298 | 0.90418 | 2.62643 | 2.98255 | 7.22268 | 7.62915 | 6.55522 | 8.8362 | 4.27901 | 1.10026 | 3.25677 | 1.50968 | 3.11888 |
| (Gd/Yb)n | 0.61113 | 0.88522 | 0.78 | 0.94876 | 0.72719 | 0.64389 | 0.61048 | 0.58239 | 0.66148 | 0.81851 | 0.73664 | 0.78054 | 0.68913 |
| (La/Sm)n | 2.45266 | 0.80131 | 1.67541 | 1.54659 | 2.02954 | 3.12236 | 2.94946 | 2.76339 | 1.95148 | 1.15126 | 2.05184 | 0.89652 | 1.66144 |
| Eu/Eu* | 1.10528 | 0.93958 | 1.14704 | 0.97107 | 1.02756 | 1.05536 | 0.95345 | 0.98632 | 0.96344 | 0.7467 | 1.06471 | 1.0753 | 1.04587 |

**INDEX**


KNOWLEDGE, TRUTH AND EXCELLENCE